

Secure SWIPT in the Multiuser STAR-RIS Aided MISO Rate Splitting Downlink

Hamid Reza Hashempour, Hamed Bastami, Majid Moradikia, Seyed A.Zekavat, *Senior Member, IEEE*,
Hamid Behroozi, *Member, IEEE*, Gilberto Berardinelli, *Senior Member, IEEE* and A. Lee Swindlehurst, *Fellow, IEEE*

Abstract—Recently, simultaneously transmitting and reflecting reconfigurable intelligent surfaces (STAR-RISs) have emerged as a novel technology that provides 360° coverage and new degrees-of-freedom (DoFs). They are also capable of manipulating signal propagation and simultaneous wireless information and power transfer (SWIPT). This paper introduces a novel STAR-RIS-aided secure SWIPT system for downlink multiple input single output rate-splitting multiple access (RSMA) networks. The transmitter concurrently communicates with the information receivers (IRs) and sends energy to untrusted energy receivers (UERs). The UERs are also capable of wiretapping the IR streams. We assume that the channel state information (CSI) of the IRs is known at the information transmitter, but only imperfect CSI for the UERs is available at the energy transmitter. By exploiting RSMA, the base station splits the messages of the IRs into common and private parts. The former is encoded into a common stream that can be decoded by all IRs, while the private messages are individually decoded by their respective IRs. We find the precoders and STAR-RIS configuration that maximizes the achievable worst-case sum secrecy rate of the IRs under a total transmit power constraint, a sum energy constraint for the UERs, and subject to constraints on the transmission and reflection coefficients. The formulated problem is non-convex and has intricately coupled variables. To tackle this challenge, a sub-optimal two-step iterative algorithm based on the sequential parametric convex approximation method is proposed. Simulations demonstrate that the RSMA-based algorithm implemented with a STAR-RIS enhances both the rate of confidential information transmission and the total spectral efficiency. Furthermore, our method surpasses the performance of both orthogonal multiple access (OMA) and non-OMA (NOMA).

Index Terms—Rate-Splitting, passive beamforming, reconfigurable intelligent surfaces, simultaneous transmission and reflection, physical layer security.

I. INTRODUCTION

Copyright (c) 2024 IEEE. Personal use of this material is permitted. However, permission to use this material for any other purposes must be obtained from the IEEE by sending a request to pubs-permissions@ieee.org.

Hamid Reza Hashempour and Gilberto Berardinelli are with the Department of Electronic Systems, Aalborg University, Aalborg, Denmark (e-mails: {hrh, gb}@es.aau.dk).

Hamed Bastami and Hamid Behroozi are with the Department of Electrical Engineering, Sharif University of Technology, Tehran, Iran, (e-mails: {hamed.bastami@ee., behroozi@}sharif.edu).

Majid Moradikia and Seyed A.Zekavat are with the Department of Physics, Worcester Polytechnic Institute (WPI), Worcester, MA, USA (e-mail: mmoradikia@wpi.edu; rezaz@wpi.edu).

A. Lee Swindlehurst is with the Center for Pervasive Communications and Computing, Henry Samueli School of Engineering, University of California, Irvine, CA, USA 92697 (e-mail: swindle@uci.edu).

DUE to rapid developments in metasurfaces and their corresponding fabrication technologies, reconfigurable intelligent surfaces (RISs) have emerged as promising candidates for next generation (NG) wireless networks [1]–[3]. RISs are typically constructed as planar arrays, consisting of many low-cost passive scattering elements. Ideally, each reconfigurable element can independently adjust the phase shift and amplitude of the incident wireless signals based on biasing voltages provided by a smart controller. Normally, RISs can only receive and reflect signals in one of the two 180° half planes defined by its planar structure, and thus an RIS can only serve users on one of its sides [4], [5]. However, a new type of RIS, referred to as a simultaneous transmitting/refracting and reflecting RIS (STAR-RIS) [6], has been introduced to overcome this limitation [7], [8]. By employing both electrical-polarization and magnetization currents, STAR-RISs can simultaneously reflect and transmit the incident signals [9], which leads to full-space 360° coverage. The transmission and reflection coefficients of the STAR-RIS elements can be configured for flexible deployments.

The inherent broadcast nature of wireless transmissions make them vulnerable to eavesdroppers. Physical layer security (PLS) techniques have been proposed for opportunistically exploiting the random characteristics of fading channels to mitigate the leakage of legitimate information to unintended recipients and thus to enhance the secrecy of wireless communications [10]–[13]. Most of these PLS schemes perform well when accurate channel state information is available at the Tx (CSIT) [10]–[13].

Rate splitting multiple access (RSMA) is a generalized framework combining non-orthogonal-multiple-access (NOMA) [14] and space division multiple access (SDMA), which achieves better multiplexing and spectral efficiency than NOMA and SDMA alone [15]. In RSMA, each transmitted message is split into a common and a private part, followed by linear transmit precoding (TPC) at a multi-antenna Tx and successive interference cancellation (SIC) at each receiver [15]. Most of the RSMA literature only considers wireless information transfer (WIT) via radio-frequency (RF) transmissions. However, RF signals carry not only information but also energy. Thus, this principle may also be applied for wireless power transfer (WPT) [16]. While information receivers (IRs) decode information, energy receivers (ERs) are capable of harvesting energy from the RF signals [17]. WIT and WPT are unified under the heading of simultaneous wireless information and power transfer (SWIPT), which simultaneously achieves

information and energy transmission to IRs and ERs, respectively [18], [19]. In downlink multiple input single output (MISO) SWIPT networks, the TPC has to strike a tradeoff between information rate and energy transfer [20].

In this work, motivated by the benefits of RSMA in SWIPT as well as the compelling applications of STAR-RIS, we conceive a robust and secure SWIPT-aided STAR-RIS-assisted RSMA downlink solution, in which the transmitter concurrently sends information to IRs and energy to untrusted energy receivers (UEs) in the transmission and reflection spaces of a STAR-RIS. Security is a critical issue since in principle the UEs are able to wiretap the IR streams. We also assume that the channel state information (CSI) of the IRs is known at the transmitter, but only Imperfect CSI (ICSI) is available for the UEs at the transmitter.

A. Related Works

1) *Studies on STAR-RIS Assisted Networks:* STAR-RIS-aided systems have been widely investigated both in orthogonal multiple access (OMA) and NOMA frameworks. For instance, in [21], a STAR-RIS assisted NOMA system was proposed for maximizing the sum rate by optimizing the power allocation as well as the active and passive beamforming. The coverage range of STAR-RIS-aided two-user communication networks relying on both NOMA and OMA were studied in [22]. The authors of [23] proposed a secure STAR-RIS-assisted uplink NOMA solution assuming either full or statistical CSI for the eavesdropper. In [24] resource allocation was designed for a STAR-RIS-assisted multi-carrier communication network. In [25], a power minimization problem was formulated for the joint optimization of the active beamformer at the BS and the passive transmission and reflection beamformers at the STAR-RIS. Three practical operating protocols were considered, namely energy splitting (ES), mode switching (MS), and time switching (TS). The authors of [26] explored the performance of STAR-RIS-assisted NOMA networks for transmission over Rician fading channels, assuming that the nearby and distant users respectively receive the reflected and transmitted signals from the STAR-RIS. Both exact and asymptotic expressions of the outage probability were also derived in [26]. More recently, in [27], the reflection and transmission coefficients of a STAR-RIS were optimized for ES and MS protocols to maximize the weighted sum rate of a full-duplex communication system. Finally, STAR-RIS-assisted PLS was introduced in [28] for improving the secrecy performance compared to that achievable by conventional RIS.

2) *Studies on Secure RIS-Aided SWIPT:* Liu *et al.* [29], maximized the energy efficiency in a secure RIS-aided SWIPT network by jointly optimizing the transmit beamforming vectors at the access point (AP), the artificial noise (AN) covariance matrix at the AP, and the phase shifts at the RIS. In [30], the secrecy rate was maximized in a heterogeneous SWIPT network with the aid of multiple RISs by carefully designing the transmit beamforming vector, the artificial noise vector, and reflecting coefficients under a specific quality-of-service (QoS) constraint. An RIS-aided secure multiple-input multiple-output (MIMO) SWIPT system was investigated in

[31], where the transmitter, IRs and ERs are all equipped with multiple antennas and the energy receiver may be a potential eavesdropper (*Eve*). Joint beamforming optimization was used for maximizing the secrecy rate. In [32] an RIS-assisted SWIPT MISO network was considered. Specifically, several RISs were utilized to assist in information/power transfer from the AP to multiple single-antenna IRs and ERs. The goal was to minimize the transmit power at the AP by jointly optimizing the coefficients of the RISs under specific QoS constraints for the users.

B. Motivations and Contributions

Although some of the above-mentioned research investigates STAR-RIS systems, PLS is not considered in [21]–[27]. Only [28] introduces a STAR-RIS aided secure network. On the other hand, most recent work on secure SWIPT only exploits conventional reflecting-only RISs [29]–[32] with only half-space coverage. Our motivation is to fill this knowledge-gap and to consider secure STAR-RIS aided SWIPT networks, which to date have not been studied in the literature. The main contributions of our work are summarized as follows:

- We conceive a secure MISO STAR-RIS-aided SWIPT solution for the RSMA downlink, where a multi-antenna BS serves the single-antenna IRs and UEs in the transmission and reflection spaces of the STAR-RIS, respectively. The UEs are also potential *Eves* that wiretap the channel. Moreover, we assume that the CSI of the UEs is not known at the transmitter, i.e., only the imperfectly estimated channel between the RIS and UEs is available at the BS.
- Although most work on STAR-RIS is based on OMA/NOMA comparisons, we demonstrate that RSMA can achieve better performance than OMA/NOMA, and can provide AN for UEs, which facilitates their secure communication.
- We show how to jointly optimize the active and passive beamforming vectors for maximizing the worst-case sum secrecy rate of the IRs, under realistic constraints on the total transmit power, the minimum sum energy of the UEs, as well as the RIS transmission and reflection coefficients. The resultant problem is non-convex with intricately coupled variables. To tackle this challenge, a suboptimal two-step iterative algorithm based on the sequential parametric convex approximation (SPCA) method of [33] is proposed for alternately solving for the TPCs as well as the transmission and reflection coefficients. Furthermore, an initialization algorithm is provided to search for a feasible initial point of the original problem and avoid potential failures.
- Rich simulations are provided for characterizing the proposed strategy and to demonstrate how increasing the number of STAR-RIS elements leads to dramatic improvement in the system performance. Our simulation results show that it is the combination of the RSMA-based algorithm and the STAR-RIS that improves the efficiency. Specifically, by increasing the number of RIS elements the performance of the network is drastically

enhanced. Furthermore, our method surpasses both OMA and NOMA in performance.

To summarize the aforementioned discussion, Table I presents a concise comparison of our approach with the state-of-the-art, underscoring the novel aspects of our methodology in the context of existing research.

C. Organization and Notation

The rest of this paper is organized as follows. Section II introduces the system model and preliminaries, while Section III presents the proposed Worst-Case Sum Secrecy Rate (WC-SSR) maximization method. Section IV details the steps of the proposed algorithm as well as its complexity. Then, several experiments are performed for validating the efficiency of the proposed approach in Section V. Finally, Section VI concludes the paper.

Notation: We use bold lowercase letters for vectors and bold uppercase letters for matrices. The notation $(\cdot)^T$ and $(\cdot)^H$ denote the transpose operator and the conjugate transpose operator, respectively. \Re and \Im represent the real and the imaginary parts of a complex variable, respectively. \triangleq denotes a definition. $\mathbb{R}^{N \times 1}$ and $\mathbb{C}^{N \times 1}$ denote the sets of N -dimensional real and complex vectors, respectively. $\mathbb{C}^{M \times N}$ stands for the set of $M \times N$ complex matrices. The matrix \mathbf{I}_N denotes the $N \times N$ identity matrix. $[\mathbf{x}]_m$ is the m -th element of a vector \mathbf{x} and $[\mathbf{X}]_{m,n}$ is the (m,n) -th element of a matrix \mathbf{X} . The operators $\text{Tr}(\cdot)$ and $\text{rank}(\cdot)$ denote the trace and rank of a matrix, while $\text{diag}\{\cdot\}$ constructs a diagonal matrix from its vector argument.

Table II presents the main parameters and variables associated with this study in order to enhance the readability of the paper.

II. SYSTEM MODEL AND PRELIMINARIES

A. Assumptions and Justification

Before presenting the system model, we briefly describe our main assumptions and justify them.

- We assume that users on one side of the STAR-RIS are unable to wiretap the channels of the other side. A similar assumption is made for secure transmission in an uplink NOMA network in [34].
- We assume that the users within the reflection space rely on energy harvesting while users within the transmission space are information receivers. However, their roles may also be readily reversed. It is trivial to show that a similar formulation may be obtained in the new model, hence we will not discuss this case further.
- We assume that CSI is available for the IRs, since the IRs typically have two-way interactions with the BS. Hence the CSI for the IRs will be much more accurate than for the UERs, since it can be readily estimated by the BS using uplink signals gleaned from the IRs. This is a reasonable model that takes the most dominant source of CSI error into account. We also note that this assumption is very commonly used in the literature [29]–[32].
- We assume the BS desires to send energy to potentially untrusted users, consistent with networks that provide

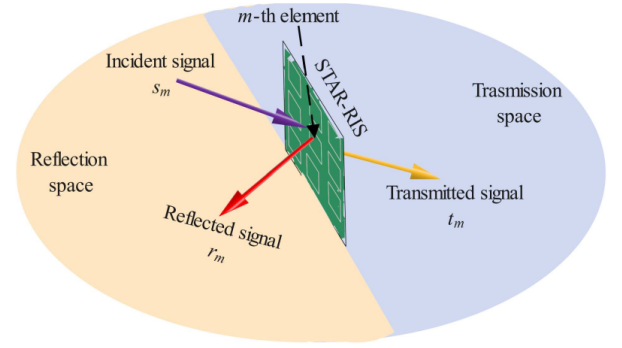


Fig. 1. Illustration of signal propagation of STAR-RISs [21]

multiple tiers of applications to their users. The network may offer different services to different users, depending for example on how much they have paid for access, or on their level of trustworthiness. For example, the network may be willing to provide energy for charging a device (e.g., in return for payment) without allowing it access to communication resources. Users who pay for communication access may desire that their communications enjoy some level of protection from unauthorized access by users who have not yet achieved a certain level of trust from the network.

B. STAR-RIS Signal Model

This section describes the signal propagation model for a STAR-RIS. Fig. 1 shows that a signal incident on a STAR-RIS element is divided into a refracted and a reflected signal in the transmission and reflection spaces, respectively. Assume that s_m is the signal incident upon the m -th RIS element, where $m \in \mathbb{M} \triangleq \{1, 2, \dots, M\}$, and M is the number of RIS elements. The signals that are transmitted and reflected by the m -th element of the RIS are respectively modelled as [21]

$$t_m = \left(\sqrt{\beta_m^t} e^{j\theta_m^t} \right) s_m \quad (1)$$

$$r_m = \left(\sqrt{\beta_m^r} e^{j\theta_m^r} \right) s_m, \quad (2)$$

where $\{\sqrt{\beta_m^t}, \sqrt{\beta_m^r} \in [0, 1]\}$ and $\{\theta_m^t, \theta_m^r \in [0, 2\pi)\}$ denote the amplitude and phase shift of the transmission and reflection coefficients of the m -th element, respectively.

We assume that the phase shifts of the transmission and reflection elements, i.e., $\{\theta_m^t, \theta_m^r\}$ do not depend on each other. However, because of the energy conservation law, the incident signal's energy has to be equal to the sum of the energies of the transmitted and reflected signals i.e., $|s_m|^2 = |t_m|^2 + |r_m|^2, \forall m \in \mathbb{M}$ and consequently we have $\beta_m^t + \beta_m^r = 1, \forall m \in \mathbb{M}$. Thus, the amplitudes of the transmission and reflection coefficients $\{\sqrt{\beta_m^t}, \sqrt{\beta_m^r}\}$ are coupled. We also assume that each STAR-RIS element operates in the energy splitting (ES) mode, i.e., simultaneous transmission and reflection mode (T & R mode) which is more general than the full transmission mode (T mode) or the full reflection mode (R mode) [6], [7]. The ES mode increases the

TABLE I
COMPARATIVE ANALYSIS OF RELATED WORKS

Keywords \ Ref.	Our Work	[21]	[22],[24]	[23]	[25]	[26]	[27]	[28]	[29],[30]	[31]	[32]
PLS	✓			✓				✓	✓	✓	
RIS									✓	✓	✓
STAR-RIS	✓	✓	✓	✓	✓	✓	✓	✓			
SWIPT	✓								✓	✓	✓
RSMA	✓										
NOMA		✓	✓	✓		✓					
OMA			✓								
WCSSR	✓							✓			
MISO	✓	✓			✓			✓	✓		✓
I-CSI	✓			✓							

TABLE II
KEY NOTATIONS USED IN THIS PAPER.

Notation	Definition
$\mathcal{K}/K/k$	Set/number/index of IRs in the transmission space
$\mathcal{J}/J/j$	Set/number/index of UERs in the reflection space
$\mathbb{M}/M/m$	Set/number/index of RIS elements
$\beta_m^t/\beta_m^r, \theta_m^t/\theta_m^r$	The amplitude and phase shift of transmission/reflection coefficients
$\mathbf{u}_t/\mathbf{u}_r, \mathbf{\Theta}_t/\mathbf{\Theta}_r$	The transmission/reflection beamforming vector and diagonal matrix
N_T	The number of transmit antennas at the BS
$\mathbf{h}_{t,k}/\mathbf{h}_{r,j}$	The combined channel of the BS to the k/j th user in the transmission/reflection space
\mathbf{H}	channel matrix from the BS to STAR-RIS
$\mathbf{g}_{t,k}/\mathbf{g}_{r,j}$	The channel vector of the RIS to the k/j th user
$\mathbf{p}_c/\mathbf{p}_k/\mathbf{f}_j$	The precoders for the common/private/energy signals of IRs/UEs
$P_t, r_c/\gamma_k$	The total available transmit power and minimum QoS requirement of common/private stream of the k th user
$\gamma_{c,k}^{\text{IR}}/\gamma_k^{\text{IR}}, \gamma_{c,j}^{\text{UER}}/\gamma_{k,j}^{\text{UER}}$	The SINR of common/private stream of the k th IR at k/j th IR/UE
$R_{c,k}/R_k, R_{c,j}^{\text{UER}}/R_{k,j}^{\text{UER}}$	The achievable rates of common/private stream of k th IR at UER- j
$R_{\text{sec},k}^{\text{tot}}$	The achievable secrecy rate between the BS-RIS and each legitimate user IR- k

number of degrees of freedom (DoFs) provided by the RIS for optimizing the network, but it also correspondingly increases the communication overhead between the BS and RIS [25].

To simplify the notation, we represent the transmission/reflection beamforming vector by $\mathbf{u}_p = [\sqrt{\beta_1^p}e^{j\theta_1^p}, \sqrt{\beta_2^p}e^{j\theta_2^p}, \dots, \sqrt{\beta_M^p}e^{j\theta_M^p}]$, where $p = t$ and $p = r$ distinguish either the beamformer is for transmission or reflection, respectively, and the corresponding diagonal transmission/reflection matrix of the STAR-RIS is given by $\mathbf{\Theta}_p = \text{diag}(\mathbf{u}_p)$. Equation (3) summarizes the set of constraints for the transmission and reflection coefficients.

C. System Model

We consider downlink transmission in a STAR-RIS assisted SWIPT network, where the direct links between the BS and single-antenna users are blocked and the BS communicates with the users only with the aid of the STAR-RIS. We denote the number of transmit antennas at the BS and the number of STAR-RIS elements by N_T and M respectively. The users are divided into two types: The IRs in the transmission space of the RIS and the UERs in the reflection area, as shown in Fig. 2. The K single-antenna IRs are indexed by $\mathcal{K} = \{1, \dots, K\}$ and the J single-antenna UERs are indexed by $\mathcal{J} = \{1, \dots, J\}$. The IRs and UERs are respectively assumed to possess Information Decoding (ID) and Energy Harvesting (EH) capabilities.

The combined channel of the BS-RIS-user link for user n for either the IRs or UERs is denoted by $\mathbf{h}_{c,n} = \mathbf{g}_{c,n}^H \mathbf{\Theta}_n \mathbf{H}$, where $\mathbf{H} \in \mathbb{C}^{M \times N_T}$ represents the channel matrix of the link from the BS to the RIS, and $\mathbf{g}_{c,n} \in \mathbb{C}^{M \times 1}$ is the channel vector of the link from the RIS to user n which is defined as

$$\mathbf{g}_{c,n} = \begin{cases} \mathbf{g}_{t,k}, & \text{if user } n \text{ is located in the transmission space} \\ \mathbf{g}_{r,j}, & \text{if user } n \text{ is located in the reflection space.} \end{cases} \quad (4)$$

The CSI of the IRs is assumed to be known at the transmitter. However, due to lack of frequent and steady interaction between the BS and UERs, the CSI of the UERs may become outdated during the transmission. Therefore, the BS only has access to the estimates $\hat{\mathbf{g}}_{r,j}$ of the channel between the BS and UERs. We use a bounded error model [35], [36] to account for the imprecise CSI of the UERs, as follows:

$$\mathbf{g}_{r,j} = \hat{\mathbf{g}}_{r,j} + \Delta \mathbf{g}_{r,j},$$

$$\Theta_g \triangleq \{\Delta \mathbf{g}_{r,j} \in \mathbb{C}^{M \times 1} : \|\Delta \mathbf{g}_{r,j}\|^2 \leq \nu^2\}, \quad (5)$$

where $\hat{\mathbf{g}}_{r,j} \in \mathbb{C}^{M \times 1}$ is the estimate of the channel between the RIS and the UERs, which is available to the BS, and $\Delta \mathbf{g}$ represents the unknown channel uncertainty of the UERs. The variable $\nu > 0$ denotes the size of the uncertainty region of the estimated UER CSI. The special case of perfect CSI for the RIS to UER channels occurs when $\nu = 0$. The diagonal matrix $\mathbf{\Theta}_n$ of RIS coefficients and the combined channel $\mathbf{h}_{c,n}$

$$\mathbb{R}_{\beta,\theta} = \{\beta_m^t, \beta_m^r, \theta_m^t, \theta_m^r \mid \beta_m^t, \beta_m^r \in [0, 1]; \beta_m^t + \beta_m^r = 1; \theta_m^t, \theta_m^r \in [0, 2\pi)\}.$$

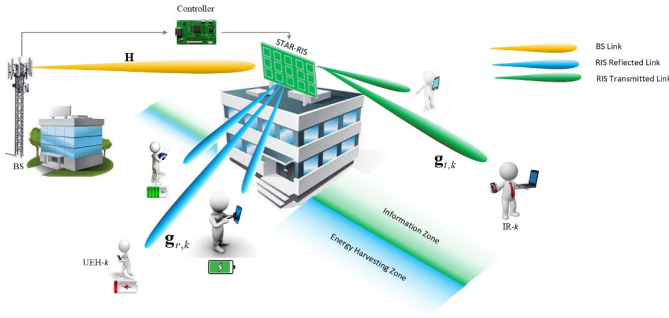


Fig. 2. System model

are respectively defined as

$$\Theta_n = \begin{cases} \Theta_t, & \text{if user } n \text{ is located in the IR space} \\ \Theta_r, & \text{if user } n \text{ is located in the UER space,} \end{cases} \quad (6)$$

$$\mathbf{h}_{c,n} = \begin{cases} \mathbf{h}_{t,k}, & \text{if user } n \text{ is located in the IR space} \\ \mathbf{h}_{r,j}, & \text{if user } n \text{ is located in the UER space.} \end{cases} \quad (7)$$

As assumed in the literature on RSMA [15], [37], [38], the BS divides the message W_k of IR- k into a common part $W_{c,k}$ and a private part $W_{p,k}$, $\forall k \in \mathcal{K}$. The common stream s_c^{ID} is created by jointly encoding the common parts of all IRs $\{W_{c,1}, \dots, W_{c,K}\}$. The private streams $\{s_1^{\text{ID}}, \dots, s_K^{\text{ID}}\}$ are obtained by independently encoding the private parts of the IRs. Therefore, the aggregated transmit signal is given by

$$\mathbf{x} = \mathbf{x}^{\text{ID}} + \mathbf{x}^{\text{EH}} = \mathbf{p}_c s_c^{\text{ID}} + \sum_{k \in \mathcal{K}} \mathbf{p}_k s_k^{\text{ID}} + \sum_{j \in \mathcal{J}} \mathbf{f}_j s_j^{\text{EH}}, \quad (8)$$

where $\mathbf{p}_c, \mathbf{p}_k$, and $\mathbf{f}_j \in \mathbb{C}^{N_T \times 1}$ are the precoders for the common, the private and the energy signals, respectively. We denote by $\mathbf{P} = [\mathbf{p}_c, \mathbf{p}_1, \dots, \mathbf{p}_K]$ and $\mathbf{F} = [\mathbf{f}_1, \dots, \mathbf{f}_J]$ the information precoder and energy precoder matrices, respectively. The sets $\mathbf{s}^{\text{ID}} = [s_c^{\text{ID}}, s_1^{\text{ID}}, \dots, s_K^{\text{ID}}]^T \in \mathbb{C}^{(K+1) \times 1}$ and $\mathbf{s}^{\text{EH}} = [s_1^{\text{EH}}, \dots, s_J^{\text{EH}}]^T \in \mathbb{C}^{J \times 1}$ represent the IR and UER streams, respectively. Under the assumption that $\mathbb{E}\{\mathbf{s}^{\text{ID}}(\mathbf{s}^{\text{ID}})^H\} = \mathbf{I}_K$ and $\mathbb{E}\{\mathbf{s}^{\text{EH}}(\mathbf{s}^{\text{EH}})^H\} = \mathbf{I}_J$, the transmit power constraint is $\text{Tr}(\mathbf{P}\mathbf{P}^H) + \text{Tr}(\mathbf{F}\mathbf{F}^H) \leq P_t$, where P_t is the total transmit power available.

The signals received at IR- k and UER- j are respectively given by

$$\begin{aligned} y_k^{\text{ID}} &= \mathbf{h}_{t,k} \mathbf{x} + n_k^{\text{ID}}, \quad \forall k \in \mathcal{K}, \\ y_j^{\text{EH}} &= \mathbf{h}_{r,j} \mathbf{x} + n_j^{\text{EH}}, \quad \forall j \in \mathcal{J}, \end{aligned} \quad (9)$$

where $\mathbf{h}_{t,k}, \mathbf{h}_{r,j} \in \mathbb{C}^{1 \times M}$ are the corresponding combined channels from the BS-RIS to IR- k and from the BS-RIS to UER- j , respectively. The terms n_k^{ID} and n_j^{EH} represent additive Gaussian noise with zero mean and unit variance received at IR- k and UER- j , respectively.

We assume that the energy precoder \mathbf{F} is perfectly known

at the transmitter and IRs, and thus the IRs remove the interference of the energy signals from y_k^{ID} to decode the desired information signals. According to the standard RSMA decoding order [15], [37], [38], before decoding the intended private stream, the common stream is decoded by each IR, while treating the private streams as interference. Hence, the Signal-to-Interference-plus-Noise Ratio (SINR) experienced upon decoding the common stream s_c^{ID} at IR- k is given by

$$\gamma_{c,k}^{\text{IR}} = \frac{|\mathbf{h}_{t,k} \mathbf{p}_c|^2}{\sum_{k' \in \mathcal{K}} |\mathbf{h}_{t,k} \mathbf{p}_{k'}|^2 + \sum_{j \in \mathcal{J}} |\mathbf{h}_{t,k} \mathbf{f}_j|^2 + 1}, \quad \forall k \in \mathcal{K}. \quad (10)$$

The contribution of s_c^{ID} is removed from y_k after decoding. Then, the intended private stream s_k^{ID} of IR- k can be decoded by treating the interference arriving from other IRs as noise. The SINR for decoding the private stream s_k^{ID} at IR- k is formulated as:

$$\gamma_k^{\text{IR}} = \frac{|\mathbf{h}_{t,k} \mathbf{p}_k|^2}{\sum_{k' \in \mathcal{K}, k' \neq k} |\mathbf{h}_{t,k} \mathbf{p}_{k'}|^2 + \sum_{j \in \mathcal{J}} |\mathbf{h}_{t,k} \mathbf{f}_j|^2 + 1}, \quad \forall k \in \mathcal{K}. \quad (11)$$

The achievable information rates of s_c^{ID} and s_k^{ID} at IR- k can be respectively written as:

$$R_{c,k} = \log_2(1 + \gamma_{c,k}^{\text{IR}}), \quad \forall k \in \mathcal{K} \quad (12)$$

$$R_k = \log_2(1 + \gamma_k^{\text{IR}}), \quad \forall k \in \mathcal{K}. \quad (13)$$

Since it is required that all IRs decode the common stream, the achievable rate of s_c^{ID} must not exceed the minimum achievable rate of all IRs, i.e., $R_c = \min\{R_{c,1}, \dots, R_{c,K}\}$. Assume that the common rate R_c is shared by all K IRs, and let C_k denote the specific portion of R_c due to transmitting $W_{c,k}$, so that we have $C_k = \alpha_k R_c$ where $\sum_{k=1}^K \alpha_k = 1$. Therefore, the overall achievable rate of IR- k is given by $R_{k,\text{tot}} = C_k + R_k$, which includes the contributions of the common and private rates $W_{c,k}$ and $W_{p,k}$, respectively.

The total harvested energy at UER- j is the sum of the energy carried by all information and energy precoders, which can be written as [39]:

$$Q_j = \zeta \left(|\mathbf{h}_{r,j} \mathbf{p}_c|^2 + \sum_{k' \in \mathcal{K}} |\mathbf{h}_{r,j} \mathbf{p}_{k'}|^2 + \sum_{j \in \mathcal{J}} |\mathbf{h}_{r,j} \mathbf{f}_j|^2 \right), \quad \forall j \in \mathcal{J}, \quad (14)$$

where $0 \leq \zeta \leq 1$ is the energy harvesting efficiency. We assume having $\zeta = 1$ in the rest of the paper.

It is assumed that the UERs are potential eavesdroppers that can wiretap the IR channels and that know the precoder matrices \mathbf{P} and \mathbf{F} . Thus, the SINR for decoding the common

stream s_c^{ID} and the private stream s_k^{ID} at UER- j are:

$$\gamma_{c,j}^{\text{UER}} = \frac{|\mathbf{h}_{r,j}\mathbf{p}_c|^2}{\sum_{k' \in \mathcal{K}} |\mathbf{h}_{r,j}\mathbf{p}_{k'}|^2 + \sum_{j' \in \mathcal{J}} |\mathbf{h}_{r,j}\mathbf{f}_{j'}|^2 + 1}, \forall j \in \mathcal{J} \quad (15)$$

$$\gamma_{k,j}^{\text{UER}} = \frac{|\mathbf{h}_{r,j}\mathbf{p}_k|^2}{|\mathbf{h}_{r,j}\mathbf{p}_c|^2 + \sum_{k' \in \mathcal{K}, k' \neq k} |\mathbf{h}_{r,j}\mathbf{p}_{k'}|^2 + \sum_{j' \in \mathcal{J}} |\mathbf{h}_{r,j}\mathbf{f}_{j'}|^2 + 1}, \quad \forall k \in \mathcal{K}, j \in \mathcal{J}. \quad (16)$$

The corresponding rates for s_c^{ID} and s_k^{ID} achievable at UER- j are $R_{c,j}^{\text{UER}} = \log_2(1 + \gamma_{c,j}^{\text{UER}})$, and $R_{k,j}^{\text{UER}} = \log_2(1 + \gamma_{k,j}^{\text{UER}})$. For the UER, we aim for designing the transmission power to ensure that the information messages are not decodable at the UER. In order to achieve this goal, the condition $\max_{j \in \mathcal{J}} \left\{ \max_{\Delta \mathbf{g}_{r,j}} \{R_{c,j}^{\text{UER}}\} \right\} < R_c$ should be satisfied for the common signal.

We emphasize that we assume a worst-case scenario in terms of security, where the UER knows both its own CSI and that of all precoders. Thus, the achievable secrecy rate between the BS-RIS and each legitimate user IR- k is given by:

$$\begin{aligned} R_{sec,k}^{\text{tot}} &\triangleq R_{sec,c} + R_{sec,k}, \quad \forall k \in \mathcal{K} \\ R_{sec,c} &\triangleq \alpha_k \left[R_c - \max_{j \in \mathcal{J}} \{R_{c,j}^{\text{UER}}\} \right]^+, \\ R_{sec,k} &\triangleq \left[R_k - \max_{j \in \mathcal{J}} \{R_{k,j}^{\text{UER}}\} \right]^+, \quad \forall k \in \mathcal{K} \end{aligned} \quad (17)$$

where we define the operation $[x]^+ \triangleq \max(0, x)$. Since the CSI between the BS and UERs is imperfectly known, the actual secrecy rate between the BS-RIS and each legitimate user IR- k for the worst case UER CSI estimation error is defined as:

$$\begin{aligned} \hat{R}_{sec,k}^{\text{tot}} &\triangleq \hat{R}_{sec,c} + \hat{R}_{sec,k}, \quad \forall k \in \mathcal{K} \\ \hat{R}_{sec,c} &\triangleq \alpha_k \left[R_c - \max_{j \in \mathcal{J}} \left\{ \max_{\Delta \mathbf{g}_{r,j}} \{R_{c,j}^{\text{UER}}\} \right\} \right]^+, \\ \hat{R}_{sec,k} &\triangleq \left[R_k - \max_{j \in \mathcal{J}} \left\{ \max_{\Delta \mathbf{g}_{r,j}} \{R_{k,j}^{\text{UER}}\} \right\} \right]^+. \end{aligned} \quad (18)$$

III. PROPOSED WCSSR MAXIMIZATION

A. Problem Formulation

Before proceeding further, we have provided a diagram, depicted in Fig. 3, to show the flow of the analysis described in the sequel.

Our objective is to maximize the WCSSR of all users with proportional rate constraints. Mathematically, the WCSSR maximization problem can be formulated as follows:

$$\max_{\mathbf{P}, \mathbf{F}, \mathbf{u}_p, \alpha} \left(\min_k \left\{ \hat{R}_{sec,k}^{\text{tot}} \right\} \right), \quad (19a)$$

$$\text{s.t. } 0 \leq \alpha_k \leq 1, \quad \forall k \in \mathcal{K}, \quad (19b)$$

$$\sum_{k \in \mathcal{K}} \alpha_k = 1, \quad (19c)$$

Step 0. Main Objective

Maximize the WCSSR of all users (18)

Step 1. Problem Formulation

WCSSR maximization problem can be posed as (19)

Step 2. Splitting the Problem to two sub-problems

Problem (19) is hard to solve because of the nonconvex objective function and the non-convex constraints. To circumvent the non-convexity, we split the problem to two sub-problems and resort to SPCA where the problem is iteratively approximated by a sequence of convex programs

Step 3. SPCA-based Solution for Precoder Optimization

First, we assume that the STAR-RIS beamforming vector is known and we optimize the precoder vectors \mathbf{P} and \mathbf{F} with SPCA as shown in Algorithm 1

Step 4. Initialization Method

In order to avoid failing initially due to infeasibility, we provide a feasible initial point search algorithm FIPSA as in Algorithm 2

Step 5. SPCA-based Solution for Beamforming Optimization

For any given precoder vector, the optimization problem for the STAR-RIS beamforming vector is reformulated as (39) and solved based on SPCA as shown in Algorithm 3

Step 6. Repeating Step 3 to 5 until convergence

Repeating the proposed two-step iterative algorithm to solve the original problem (19) according to Algorithm (4)

Fig. 3. Analyzing the problem: A step-by-step overview

$$R_c \leq R_{c,k}, \quad \forall k \in \mathcal{K}, \quad (19d)$$

$$\alpha_k R_c \geq r_c, \quad \forall k \in \mathcal{K} \quad (19e)$$

$$\sum_{j \in \mathcal{J}} \min_{\Delta \mathbf{g}_{r,j}} \{Q_j\} \geq E^{th}, \quad (19f)$$

$$\text{Tr}(\mathbf{P}\mathbf{P}^H) + \text{Tr}(\mathbf{F}\mathbf{F}^H) \leq P_t, \quad (19g)$$

$$\beta_m^p, \theta_m^p \in \mathbb{R}_{\beta, \theta}, \quad \forall m \in \mathbb{M}, \quad \forall p \in \{t, r\}, \quad (19h)$$

where r_c is a predefined threshold, $\alpha \triangleq [\alpha_1, \alpha_2, \dots, \alpha_K]^T$, and E^{th} is a threshold representing the minimum harvested energy required by the UERs. Note that in constraint (19f), we use the worst-case scenario for the sum of the energy harvested by the UERs due to the imperfect CSI of the link between the RIS and the UERs. Problem (19) is difficult to solve because of the nonconvex nature of the objective function and the non-convex constraints. Thus, finding the global optimum is generally intractable. To circumvent the non-convexity, we resort to SPCA, where the problem is iteratively approximated by a sequence of convex programs. At each iteration, the non-convex constraints are replaced by convex surrogates that serve as approximations.

B. SPCA-based Solution for Precoder Optimization

We assume here that the STAR-RIS beamforming vector \mathbf{u}_p is known and we want to optimize the precoders \mathbf{P}, \mathbf{F} . To use SPCA, we first mitigate the non-convexity using some variable transformations and linearization. Then, a well-suited convex subset is constructed via SPCA that approximates the original

non-convex solution set. We adopt an iterative solution to cope with the nonconvexity by approximating the non-convex factor at each iteration by its first order Taylor expansion. In what follows, we independently examine each non-convex term and derive its convex counterpart.

1) *Non-Convex Objective Function* (19a): We first eliminate the inner minimization of the max-min problem (19) that finds the worst-case CSI model in the bounded set. To do so, we introduce the auxiliary variable r_{sec} and reformulate the objective together with the constraints of (19) as follows:

$$\begin{aligned} & \max_{\mathbf{P}, \mathbf{F}, \alpha} r_{sec} \quad (20a) \\ \text{s.t. } & \alpha_k \left[R_c - \max_{j \in \mathcal{J}} \left\{ \max_{\Delta \mathbf{g}_{r,j}} \{R_{c,j}^{\text{UER}}\} \right\} \right]^+ + \\ & \left[R_k - \max_{j \in \mathcal{J}} \left\{ \max_{\Delta \mathbf{g}_{r,j}} \{R_{k,j}^{\text{UER}}\} \right\} \right]^+ \geq r_{sec}, \quad \forall k \in \mathcal{K} \quad (20b) \\ & (19b) - (19g). \quad (20c) \end{aligned}$$

It can be seen that r_{sec} plays the role of a lower bound for $\min_k \{\hat{R}_{sec,k}^{\text{tot}}\}$, and its maximization will increase the left-side of the constraint (20b), so that the constraint is active at the optimum. We note that to arrive at (20), $\hat{R}_{sec,c}$ and $\hat{R}_{sec,k}$ in (20b) were substituted by their definitions from (18).

Due to the operator $[\cdot]^+$, the constraint (20b) is nonconvex. We will relax the problem by introducing two artificial constraints in (21e) and (21f) to replace this operator. To further facilitate convexifying (20), we define two sets of new auxiliary variables $\alpha_c \triangleq [\alpha_{c,1}, \alpha_{c,2}, \dots, \alpha_{c,J}]^T$ and $\alpha_p \triangleq [\alpha_{p,1}, \alpha_{p,2}, \dots, \alpha_{p,K}]^T$, where $\alpha_{p,k} \triangleq [\alpha_{p,k,1}, \alpha_{p,k,2}, \dots, \alpha_{p,k,J}]^T$, $\forall k \in \mathcal{K}$. This allows us to transform (20) into:

$$\begin{aligned} & \max_{\mathbf{P}, \mathbf{F}, \alpha, \alpha_c, \alpha_p} r_{sec} \quad (21a) \\ \text{s.t. } & \alpha_k (R_c - \alpha_{c,j}) + \gamma_k - \alpha_{p,k,j} \geq r_{sec}, \quad \forall k \in \mathcal{K}, \quad (21b) \\ & \max_{\Delta \mathbf{g}_{r,j}} \{R_{c,j}^{\text{UER}}\} \leq \alpha_{c,j}, \quad \forall j \in \mathcal{J}, \quad (21c) \\ & \max_{\Delta \mathbf{g}_{r,j}} \{R_{k,j}^{\text{UER}}\} \leq \alpha_{p,k,j}, \quad \forall j \in \mathcal{J}, \quad (21d) \\ & R_c \geq \alpha_{c,j}, \quad \forall j \in \mathcal{J}, \quad (21e) \\ & \gamma_k \geq \alpha_{p,k,j}, \quad \forall j \in \mathcal{J}, k \in \mathcal{K}, \quad (21f) \\ & \gamma_k \leq R_k, \quad \forall k \in \mathcal{K}, \quad (21g) \\ & (19b) - (19g). \quad (21h) \end{aligned}$$

Based on the above discussion, γ_k represents a lower-bound for R_k , while $\alpha_{c,j}$ and $\alpha_{p,k,j}$ serve as upper-bounds for $\max_{j \in \mathcal{J}} \left\{ \max_{\Delta \mathbf{g}_{r,j}} \{R_{c,j}^{\text{UER}}\} \right\}$ and $\max_{j \in \mathcal{J}} \left\{ \max_{\Delta \mathbf{g}_{r,j}} \{R_{k,j}^{\text{UER}}\} \right\}$, respectively. Increasing the lower-bound and simultaneously reducing the upper-bounds boosts the left-side of the constraints, which makes the constraints (21b)-(21g) active at the optimum.

Despite this linearization, it can be seen by invoking the definitions of $R_{c,j}^{\text{UER}}$, $R_{k,j}^{\text{UER}}$ and R_k that the constraints (21b)-(21d), and (21g) are still non-convex. To handle the non-convexity of these constraints, we construct a suitable inner

convex subset for approximating the nonconvex feasible solution set. Along this line, we first approximate (21b) by its first-order Taylor expansion to obtain

$$\Theta^{[i]}(\alpha_k, R_c) - \bar{\Theta}^{[i]}(\alpha_k, \alpha_{c,j}) + \gamma_k - \alpha_{p,k,j} \geq r_{sec}, \quad (22)$$

where we have defined

$$\begin{aligned} \Theta^{[i]}(x, y) & \triangleq \quad (23) \\ & \frac{1}{2}(x^{[i]} + y^{[i]})(x + y) - \frac{1}{4}(x^{[i]} + y^{[i]})^2 - \frac{1}{4}(x - y)^2, \end{aligned}$$

and

$$\begin{aligned} \bar{\Theta}^{[i]}(x, y) & \triangleq \quad (24) \\ & \frac{1}{4}(x + y)^2 + \frac{1}{4}(x^{[i]} - y^{[i]})^2 - \frac{1}{2}(x^{[i]} - y^{[i]})(x - y) \end{aligned}$$

for the linear approximation of the terms, which involve the product of two variables.

To handle the non-convexity of (21c), (21d), and (21g) we build a suitable inner convex subset to approximate the nonconvex feasible solution set. In particular, we first define a set of new auxiliary variables $\pi_{c,j,j',k} \triangleq [\rho_{c,j}, \rho_{k,j}, \rho_k, a_{j,k}, b_{j,j'}, x_{c,j}, x_{k,j}, v_j]$, $\forall k \in \mathcal{K}, \{j, j'\} \in \mathcal{J}$ and exploit the following Propositions.

Proposition 1. An affine approximation of constraint (21c), $\forall j \in \mathcal{J}$ is given by:

$$\begin{cases} \text{(I)} : 1 + \rho_{c,j} - \Gamma^{[i]}(\alpha_{c,j}) \leq 0, \\ \text{(II)} : \frac{x_{c,j}^2}{\sum_{k' \in \mathcal{K}} a_{j,k'} + \sum_{j' \in \mathcal{J}} b_{j,j'} + 1} \leq \rho_{c,j}, \\ \text{(III)} : |\hat{\mathbf{g}}_{r,j}^H \mathbf{p}'_c| + \nu \|\mathbf{p}'_c\|_2 \leq x_{c,j}, \\ \text{(IV)} : \text{Tr}[(\hat{\mathbf{G}}_{r,j} - \mu_j \mathbf{I}) \mathbf{P}'_{k'}] \geq a_{j,k'}, \\ \text{(V)} : \text{Tr}[(\hat{\mathbf{G}}_{r,j} - \mu_j \mathbf{I}) \mathbf{F}'_{j'}] \geq b_{j,j'}, \end{cases} \quad (25)$$

where

$$\Gamma^{[i]}(x) \triangleq 2^{x^{[i]}} [1 + \ln(2)(x - x^{[i]})], \quad (26)$$

$$\hat{\mathbf{G}}_{r,j} \triangleq \hat{\mathbf{g}}_{r,j} \hat{\mathbf{g}}_{r,j}^H, \quad (27)$$

$$\mathbf{P}'_{k'} \triangleq \mathbf{p}'_{k'} (\mathbf{p}'_{k'})^H, \quad (28)$$

$$\mathbf{p}'_n \triangleq \Theta_r \mathbf{H} \mathbf{p}_n, \text{ for } n \in \{c, k\}, \quad (29)$$

$$\mathbf{F}'_{j'} \triangleq \mathbf{f}'_{j'} (\mathbf{f}'_{j'})^H, \quad (30)$$

$$\mu_j \triangleq \nu^2 + 2\nu \|\hat{\mathbf{g}}_{r,j}\|_2. \quad (31)$$

Proof. See Appendix A. ■

Proposition 2. An affine approximation of constraint (21d), $\forall j \in \mathcal{J}, k \in \mathcal{K}$ is given by:

$$\begin{cases} \text{(I)} : 1 + \rho_{k,j} - \Gamma^{[i]}(\alpha_{p,k,j}) \leq 0, \\ \text{(II)} : \frac{x_{k,j}^2}{v_j + \sum_{k' \in \mathcal{K}, k' \neq k} a_{j,k'} + \sum_{j' \in \mathcal{J}} b_{j,j'} + 1} \leq \rho_{k,j}, \\ \text{(III)} : |\hat{\mathbf{g}}_{r,j}^H \mathbf{p}'_k| + \nu \|\mathbf{p}'_k\|_2 \leq x_{k,j}, \\ \text{(IV)} : \text{Tr}[(\hat{\mathbf{G}}_{r,j} - \mu_j \mathbf{I}) \mathbf{P}'_c] \geq v_j, \end{cases} \quad (32)$$

where $\mathbf{P}'_c \triangleq \mathbf{p}'_c (\mathbf{p}'_c)^H$.

Proof. This Proposition can be proved following the same approach as that presented in Appendix A. ■

Proposition 3. An affine approximation of constraint (21g), $\forall k \in \mathcal{K}$ is given by:

$$\begin{cases} \text{(I)} : 1 + \rho_k - 2^{\gamma_k} \geq 0, \\ \text{(II)} : \sum_{k' \in \mathcal{K}, k' \neq k} |\mathbf{h}_{t,k} \mathbf{p}_{k'}|^2 + \sum_{j \in \mathcal{J}} |\mathbf{h}_{t,k} \mathbf{f}_j|^2 - \Psi^{[i]}(\mathbf{p}_k, \rho_k; \mathbf{h}_{t,k}) + 1 \leq 0, \end{cases} \quad (33)$$

where $\Psi^{[i]}(\mathbf{u}, x; \mathbf{h}) \triangleq \frac{2^{\Re\{\mathbf{u}^{[i]H} \mathbf{h} \mathbf{h}^H \mathbf{u}\}}}{x^{[i]}} - \frac{|\mathbf{h}^H \mathbf{u}^{[i]}|^2 x}{(x^{[i]})^2}$.

Proof. See Appendix B. ■

2) *Non-convex constraint (19d):* To handle the nonconvexity of (19d), we first introduce the new auxiliary variables $\rho_{c,k} \forall k \in \mathcal{K}$ and resort to Proposition 4, as follows:

Proposition 4. An affine approximation of constraint (19d), $\forall k \in \mathcal{K}$ is given by:

$$\begin{cases} \text{(I)} : 1 + \rho_{c,k} - 2^{R_c} \geq 0, \\ \text{(II)} : \sum_{k' \in \mathcal{K}} |\mathbf{h}_{t,k} \mathbf{p}_{k'}|^2 + \sum_{j \in \mathcal{J}} |\mathbf{h}_{t,k} \mathbf{f}_j|^2 - \Psi^{[i]}(\mathbf{p}_c, \rho_{c,k}; \mathbf{h}_{t,k}) + 1 \leq 0. \end{cases} \quad (34)$$

Proof. This Proposition is proved by following the same approach as that presented in Appendix B. ■

3) *Non-convex constraint (19e):* To handle the nonconvexity of (19e), we utilize Proposition 5, as follows:

Proposition 5. An affine approximation of constraint (19e), $\forall k \in \mathcal{K}$ is given by:

$$\Theta^{[i]}(\alpha_k, R_c) \geq r_c. \quad (35)$$

Proof. See Appendix C. ■

4) *Non-convex constraint (19f):* To handle the nonconvexity of (19f), we introduce the new auxiliary variables $\lambda_{c,j,j',k} \triangleq [\lambda_{j,c}, \lambda_{j,k}, \xi_{j,j'}]$, $\forall k \in \mathcal{K}, \{j, j'\} \in \mathcal{J}$ and use the following Proposition:

Proposition 6. An affine approximation of constraint (19f), is given by:

$$\begin{cases} \text{(I)} : \sum_{j \in \mathcal{J}} \left(\lambda_{j,c} + \sum_{k \in \mathcal{K}} \lambda_{j,k} + \sum_{j' \in \mathcal{J}} \xi_{j,j'} \right) \geq E^{th}, \\ \text{(II)} : \text{Tr} \left[(\hat{\mathbf{G}}_{r,j} - \mu_j \mathbf{I}) \mathbf{P}'_c \right] \geq \lambda_{j,c}, \forall j \in \mathcal{J}, \\ \text{(III)} : \text{Tr} \left[(\hat{\mathbf{G}}_{r,j} - \mu_j \mathbf{I}) \mathbf{P}'_k \right] \geq \lambda_{j,k}, \forall j \in \mathcal{J}, k \in \mathcal{K}, \\ \text{(IV)} : \text{Tr} \left[(\hat{\mathbf{G}}_{r,j} - \mu_j \mathbf{I}) \mathbf{F}'_{j'} \right] \geq \xi_{j,j'}, \forall j, j' \in \mathcal{J}. \end{cases} \quad (36)$$

Proof. See Appendix D. ■

With the above approximations, the proposed SPCA-based approach is outlined in Algorithm 1, in which the following convex optimization problem is solved:

$$\begin{aligned} \max_{\mathbf{x}} \quad & r_{sec} \\ \text{s.t.} \quad & (21b), (21e), (21f), (19b), (19c), \\ & (25) - (36), \bar{\omega} \geq 0 \end{aligned} \quad (37)$$

where $\bar{\omega} \triangleq [\gamma_k, \alpha_c, \alpha_p, \pi_{c,j,j',k}, \rho_{c,k}, \lambda_{c,j,j',k}]$, $\forall k \in \mathcal{K}, \{j, j'\} \in \mathcal{J}$, and $\mathbf{x} \triangleq [\mathbf{P}, \mathbf{F}, \alpha, \bar{\omega}]$. If there exist feasible initial points for (37), the feasible set defined by the constraints of (37) and consequently the resultant solutions are guaranteed to lie within the original feasible set defined by (19). The procedure continues until the stopping criterion is satisfied or the affordable number of iterations is reached.

Algorithm 1 SPCA-based Algorithm for Precoder Optimization

- 1: **Input:** Set the threshold value for accuracy (δ_I) and the maximum number of iterations (N_{max}).
 - 2: **Initialization:** Initialize $\mathbf{x}^{[i]}$ with a feasible initialization point and set $i = 0$.
 - 3: **while** $|r_{sec}^{[m+1]} - r_{sec}^{[i]}| \geq \delta_I$ or $i \leq N_{max}$ **do** (I)-(III)
 - 4: **I:** Find $\mathbf{x}^{[i+1]}$ by solving (37).
 - 5: **II:** Update the slack variables based on $\mathbf{x}^{[i+1]}$.
 - 6: **III:** $i = i + 1$.
 - 7: **end while**
 - 8: **Output:** $\mathbf{P}^*, \mathbf{F}^*$.
-

Note that if Algorithm 1 were to be initialized randomly, it may fail initially due to infeasibility. To circumvent this issue, we further provide a feasible initial point search (FIPS) in Algorithm 2. In this approach, we minimize an infeasibility indicator parameter $s > 0$ as a measure of the violation of the constraints in (37). Thus, we rewrite the constraints of (37) in the form of $\mathcal{G}_i|_{i=1}^{11} \leq s$, where \mathcal{G}_i represents the i -th constraint with all terms shifted to the left-hand side, and we formulate the feasibility problem as follows:

$$\min_{\mathbf{x}} s \quad \text{s.t.} \quad \mathcal{G}_i|_{i=1}^{11} \leq s, \quad (38)$$

Algorithm 2 FIPS Algorithm

- 1: **Input:** Set the threshold value for accuracy (δ_e) and the maximum number of iterations (M_{max}).
 - 2: **Initialization:** Choose a random initialization $\mathbf{x}^{[i]}$ and set $m = 0$.
 - 3: **while** $|s^{[i+1]} - s^{[i]}| \geq \delta_e$ or $i \leq M_{max}$ **do** (I),(II)
 - 4: **I:** Solve (38).
 - 5: **II:** $i = i + 1$.
 - 6: **end while**
 - 7: **Output:** \mathbf{x}^* .
-

The above initialization procedure was previously proposed in [41], [42] as a low-complexity scheme for efficiently finding feasible initial points. Overall, the proposed FIPS Algorithm 2 runs as the first step, and then the calculated initial points (IPs) are fed to Algorithm 1. Algorithm 2 commences with random IPs and the algorithm stops if either the stopping criterion is satisfied or the maximum number of iterations is reached. We remark that if at the i -th iteration the current objective value s is zero, the algorithm stops even if the other stopping criteria are not satisfied.

C. SPCA-based Solution for Transmission and Reflection Beamforming Optimization

For the next step, in order to simplify the optimization problem, we change the objective function to optimize the sum rate for the legitimate users. Therefore, for any given precoder vectors \mathbf{p}_c , \mathbf{p}_k , and \mathbf{f}_j , the optimization problem for the RIS beamforming vector \mathbf{u}_n is reformulated as

$$\max_{\mathbf{u}_p} \left(R_c + \sum_k \gamma_k \right), \quad (39a)$$

$$\text{s.t. } R_c \leq R_{c,k}, \quad \forall k \in \mathcal{K}, \quad (39b)$$

$$\gamma_k \leq R_k, \quad \forall k \in \mathcal{K}, \quad (39c)$$

$$\alpha_k R_c \geq r_c, \quad \forall k \in \mathcal{K}, \quad (39d)$$

$$\sum_{j \in \mathcal{J}} \min_{\Delta \mathbf{g}_{r,j}} \{Q_j\} \geq E^{th}, \quad (39e)$$

$$\beta_m^p, \theta_m^p \in \mathbb{R}_{\beta,\theta}, \quad \forall m \in \mathbb{M}, \quad \forall p \in \{t, r\}. \quad (39f)$$

Given the precoders \mathbf{p}_c , \mathbf{p}_k , and \mathbf{f}_j , we denote $\bar{\mathbf{h}}_{t,k,n} = \text{diag}(\mathbf{g}_{t,k}^H) \mathbf{H} \mathbf{p}_n$, for $n \in \{c, k\}$, $\bar{\mathbf{h}}_{t,k,j} = \text{diag}(\mathbf{g}_{t,k}^H) \mathbf{H} \mathbf{f}_j$, $\mathbf{v}_p = \mathbf{u}_p^H$, and $\mathbf{V}_p = \mathbf{v}_p \mathbf{v}_p^H$, where $\mathbf{V}_p \succeq 0$, $\text{rank}(\mathbf{V}_p) = 1$, and $[\mathbf{V}_p]_{m,m} = \beta_m^p, p \in \{t, r\}$. Hence, we have:

$$|\mathbf{h}_{t,k} \mathbf{p}_n|^2 = |\mathbf{v}_t^H \bar{\mathbf{h}}_{t,k,n}|^2 = \text{Tr}(\mathbf{V}_t \bar{\mathbf{H}}_{t,k,n}), \quad n \in \{c, k\}, \quad (40)$$

$$|\mathbf{h}_{t,k} \mathbf{f}_j|^2 = |\mathbf{v}_t^H \bar{\mathbf{h}}_{t,k,j}|^2 = \text{Tr}(\mathbf{V}_t \bar{\mathbf{H}}_{t,k,j}), \quad (41)$$

where $\bar{\mathbf{H}}_{t,k,n} = \bar{\mathbf{h}}_{t,k,n} \bar{\mathbf{h}}_{t,k,n}^H$, $n \in \{c, k, j\}$. Before solving problem (39), we also introduce a slack variable set $\{A_{c,k}, B_{c,k}, A_k, B_k | k \in \mathcal{K}\}$ defined as

$$\frac{1}{A_{c,k}} = \text{Tr}(\mathbf{V}_t \bar{\mathbf{H}}_{t,k,c}), \quad (42)$$

$$B_{c,k} = \sum_{k' \in \mathcal{K}} \text{Tr}(\mathbf{V}_t \bar{\mathbf{H}}_{t,k,k'}) + \sum_{j \in \mathcal{J}} \text{Tr}(\mathbf{V}_t \bar{\mathbf{H}}_{t,k,j}) + 1, \quad (43)$$

$$\frac{1}{A_k} = \text{Tr}(\mathbf{V}_t \bar{\mathbf{H}}_{t,k,k}), \quad (44)$$

$$B_k = \sum_{k' \in \mathcal{K}, k' \neq k} \text{Tr}(\mathbf{V}_t \bar{\mathbf{H}}_{t,k,k'}) + \sum_{j \in \mathcal{J}} \text{Tr}(\mathbf{V}_t \bar{\mathbf{H}}_{t,k,j}) + 1. \quad (45)$$

Upon substituting (42) and (43) into (10) and (44) and (45) into (11), the achievable data rates for the common and private streams, respectively, can be rewritten as

$$R_{c,k} = \log_2 \left(1 + \frac{1}{A_{c,k} B_{c,k}} \right), \quad (46)$$

$$R_k = \log_2 \left(1 + \frac{1}{A_k B_k} \right). \quad (47)$$

The surrogate constraints (46) and (47) to be used in place of (39b) and (39c) are still non-convex. However, $\log_2 \left(1 + \frac{1}{xy} \right)$ is a joint convex function with respect to x and y , so using a first-order Taylor expansion we approximate the right-hand side of (46) and (47) by the following lower bounds:

$$\log_2 \left(1 + \frac{1}{A_{c,k} B_{c,k}} \right) \geq \tilde{R}_{c,k} = \log_2 \left(1 + \frac{1}{A_{c,k}^{[l]} B_{c,k}^{[l]}} \right)$$

$$- \frac{\log_2(e)(A_{c,k} - A_{c,k}^{[l]})}{A_{c,k}^{[l]} + (A_{c,k}^{[l]})^2 B_{c,k}^{[l]}} - \frac{\log_2(e)(B_{c,k} - B_{c,k}^{[l]})}{B_{c,k}^{[l]} + (B_{c,k}^{[l]})^2 A_{c,k}^{[l]}} \quad (48)$$

$$\log_2 \left(1 + \frac{1}{A_k B_k} \right) \geq \tilde{R}_k = \log_2 \left(1 + \frac{1}{A_k^{[l]} B_k^{[l]}} \right) - \frac{\log_2(e)(A_k - A_k^{[l]})}{A_k^{[l]} + (A_k^{[l]})^2 B_k^{[l]}} - \frac{\log_2(e)(B_k - B_k^{[l]})}{B_k^{[l]} + (B_k^{[l]})^2 A_k^{[l]}}, \quad (49)$$

where $A_{c,k}^{[l]}$, $B_{c,k}^{[l]}$, $A_k^{[l]}$, and $B_k^{[l]}$ represent the values of $A_{c,k}$, $B_{c,k}$, A_k , and B_k in the l -th iteration, respectively. Thus, the transmission and reflection beamforming optimization problem in (39) assuming fixed precoders can be reformulated as

$$\max_{\mathbf{v}_p} \left(R_c + \sum_k \gamma_k \right), \quad (50a)$$

$$\text{s.t. } \frac{1}{A_{c,k}} \leq \text{Tr}(\mathbf{V}_t \bar{\mathbf{H}}_{t,k,c}), \quad (50b)$$

$$B_{c,k} \geq \sum_{k' \in \mathcal{K}} \text{Tr}(\mathbf{V}_t \bar{\mathbf{H}}_{t,k,k'}) + \sum_{j \in \mathcal{J}} \text{Tr}(\mathbf{V}_t \bar{\mathbf{H}}_{t,k,j}) + 1, \quad (50c)$$

$$\tilde{R}_{c,k} \geq R_c, \quad (50d)$$

$$\frac{1}{A_k} = \text{Tr}(\mathbf{V}_t \bar{\mathbf{H}}_{t,k,k}), \quad (50e)$$

$$B_k = \sum_{k' \in \mathcal{K}, k' \neq k} \text{Tr}(\mathbf{V}_t \bar{\mathbf{H}}_{t,k,k'}) + \sum_{j \in \mathcal{J}} \text{Tr}(\mathbf{V}_t \bar{\mathbf{H}}_{t,k,j}) + 1, \quad (50f)$$

$$\tilde{R}_k \geq R_k, \quad (50g)$$

$$\beta_m^t + \beta_m^r = 1, \quad (50h)$$

$$[\mathbf{V}_p]_{m,m} = \beta_m^p, \quad (50i)$$

$$\mathbf{V}_p \succeq 0, \quad (50j)$$

$$\text{rank}(\mathbf{V}_p) = 1, \quad (50k)$$

$$(39d), (39e), \quad (50l)$$

where $p \in \{t, r\}$, and $m \in \mathbb{M}$.

As in [43], [44], the non-convex rank-one constraint (50k) can be replaced by the following relaxed convex constraint:

$$\epsilon_{max}(\mathbf{V}_p) \geq \epsilon^{[l]} \text{Tr}(\mathbf{V}_p), \quad (51)$$

where $\epsilon_{max}(\mathbf{V}_p)$ denotes the maximum eigenvalue of matrix \mathbf{V}_p , and $\epsilon^{[l]}$ is a relaxation parameter in the l -th iteration that scales the ratio of $\epsilon_{max}(\mathbf{V}_p)$ to the trace of \mathbf{V}_p . Specifically, $\epsilon^{[l]} = 0$ indicates that the rank-one constraint is dropped, while $\epsilon^{[l]} = 1$ means it is retained. Therefore, we can increase $\epsilon^{[l]}$ from 0 to 1 with each iteration to gradually approach a rank-one solution. It is noted that $\epsilon_{max}(\mathbf{V}_p)$ is not differentiable, so we use the following expression to approximate it:

$$\epsilon_{max}(\mathbf{V}_p) \approx e_{max}^H(\mathbf{V}_p^{[l]}) \mathbf{V}_p e_{max}(\mathbf{V}_p^{[l]}), \quad (52)$$

where $e_{max}(\mathbf{V}_p^{[l]})$ is the eigenvector corresponding to the maximum eigenvalue of $\mathbf{V}_p^{[l]}$. Thus, solving problem (50) is

transformed to solving the following relaxed problem:

$$\max_{\mathbf{u}_p} \left(R_c + \sum_k \gamma_k \right), \quad (53a)$$

$$\text{s.t. } e_{max}^H(\mathbf{V}_p^{[l]}) \mathbf{V}_p e_{max}(\mathbf{V}_p^{[l]}) \geq \epsilon^{[l]} \text{Tr}(\mathbf{V}_p), \quad (53b)$$

$$(39d), (39e), (50b) - (50j). \quad (53c)$$

The parameter $\epsilon^{[l]}$ can be updated via [44]

$$\epsilon^{[l+1]} = \min \left(1, \frac{\epsilon_{max}(\mathbf{V}_p^{[l]})}{\text{Tr}(\mathbf{V}_p^{[l]})} + \Delta^{[l]} \right), \quad (54)$$

where $\Delta^{[l]}$ is the step size.

Next we address the non-convex constraints (39d) and (39e). According to Proposition 5, the affine approximation of constraint (39d) is obtained by (35). In order to deal with the non-convexity of (39e), we first modify the expression for some variables as follows:

$$|\mathbf{h}_{r,j} \mathbf{p}_n|^2 = |\mathbf{v}_r^H \bar{\mathbf{h}}_{r,j,n}|^2 = \text{Tr}(\mathbf{V}_r \bar{\mathbf{H}}_{r,j,n}), \quad (55)$$

$$|\mathbf{h}_{r,j} \mathbf{f}_j|^2 = |\mathbf{v}_r^H \bar{\mathbf{h}}_{r,j,j'}|^2 = \text{Tr}(\mathbf{V}_r \bar{\mathbf{H}}_{r,j,j'}), \quad (56)$$

where $\bar{\mathbf{h}}_{r,j,n} = \text{diag}(\mathbf{g}_{r,j}^H) \mathbf{H} \mathbf{p}_n$, $n \in \{c, k\}$, $\bar{\mathbf{h}}_{r,j,j'} = \text{diag}(\mathbf{g}_{r,j}^H) \mathbf{H} \mathbf{f}_j$, $\bar{\mathbf{H}}_{r,j,n} = \bar{\mathbf{h}}_{r,j,n} \bar{\mathbf{h}}_{r,j,n}^H$, and $\bar{\mathbf{H}}_{r,j,j'} = \bar{\mathbf{h}}_{r,j,j'} \bar{\mathbf{h}}_{r,j,j'}^H$. Then, applying the same approach as in Proposition 6 and after some simple algebraic manipulations, (39e) can be rewritten as:

$$\begin{cases} \text{(I)} : \sum_{j \in \mathcal{J}} \left(\lambda_{j,c} + \sum_{k \in \mathcal{K}} \lambda_{j,k} + \sum_{j' \in \mathcal{J}} \xi_{j,j'} \right) \geq E^{th}, \\ \text{(II)} : \text{Tr}[(\bar{\mathbf{H}}_{r,j,c} - \mu_c \mathbf{I}) \mathbf{V}_r] \geq \lambda_{j,c}, \quad \forall j \in \mathcal{J}, \\ \text{(III)} : \text{Tr}[(\bar{\mathbf{H}}_{r,j,k} - \mu_k \mathbf{I}) \mathbf{V}_r] \geq \lambda_{j,k}, \quad \forall j \in \mathcal{J}, k \in \mathcal{K}, \\ \text{(IV)} : \text{Tr}[(\bar{\mathbf{H}}_{r,j,j'} - \mu_j \mathbf{I}) \mathbf{V}_r] \geq \xi_{j,j'}, \quad \forall j, j' \in \mathcal{J}, \end{cases} \quad (57)$$

where $\mu_n = \nu^2 + 2\nu \|\bar{\mathbf{h}}_{r,j,n}\|_2$, $n \in \{c, k, j\}$. Therefore, problem (50) can finally be written as

$$\max_{\mathbf{u}_p} \left(R_c + \sum_k \gamma_k \right), \quad (58)$$

s.t. (53b), (35), (57), (50b) - (50j).

Problem (58) is a standard convex SDP, which can be solved efficiently by numerical solvers such as the SDP tool in CVX [45]. The details of the proposed sequential constraint relaxation algorithm are presented in Algorithm 3.

IV. OVERALL PROPOSED ALGORITHM, CONVERGENCE AND COMPLEXITY

Based on the above discussions, here we describe the proposed two-step iterative algorithm to solve the original problem (19) in Algorithm (4). Our approach is to alternate between optimizing the precoders and optimizing the transmission and reflection beamforming vectors.

A. Convergence Analysis

In this section we provide a convergence analysis of the proposed SPCA algorithm. Since the original problem (19) is

Algorithm 3 SPCA-based Algorithm for obtaining $\{\mathbf{V}_p^*\}$

- 1: Choose initial feasible points $\mathbf{V}_p^{[0]}$, step size $\Delta^{[0]}$, error tolerance δ_p , and set the relaxation parameter $\epsilon^{[l]} = 0$ and the iteration index $l = 0$.
- 2: **repeat**
- 3: Solve problem (58) to obtain \mathbf{V}_p ;
- 4: **if** problem (58) is solvable **then**
- 5: Update $\mathbf{V}_p^{[l+1]} = \mathbf{V}_p$;
- 6: Update $\Delta^{[l+1]} = \Delta^{[l]}$;
- 7: **else**
- 8: Update $\Delta^{[l+1]} = \Delta^{[l]}/2$;
- 9: **end if**
- 10: $l = l + 1$.
- 11: Update $\epsilon^{[l+1]}$ via (54);
- 12: **until** $|1 - \epsilon^{[l]}| \leq \delta_p$ and the objective value of problem (58) converges.
- 13: Output: \mathbf{V}_p^* .

Algorithm 4 The overall proposed Algorithm

- 1: **Input:** Set the parameters $\delta_e, \delta_p, \delta_I, N_{max}, M_{max}, \Delta^{[0]}$.
- 2: **Initialization:** Randomly initialize $\mathbf{x}^{[0]}, \mathbf{V}_p^{[0]}$, and set the relaxation parameter $\epsilon^{[l]} = 0$ and iteration indices $l = 0, i = 0$.
- 3: **repeat**
- 4: Update $\mathbf{x}^{[i]}$ via Algorithm 2;
- 5: Update the precoder vectors \mathbf{P}, \mathbf{F} via Algorithm 1;
- 6: Update the beamforming vector \mathbf{u}_p via Algorithm 3;
- 7: **until** the objective value of problem (19) converges.
- 8: Output: $\mathbf{P}^*, \mathbf{F}^*, \mathbf{V}_p^*$.

non-convex, it is not possible to prove convergence to a global minimum, but convergence to Karush-Kuhn-Tucker (KKT) points under some regularity conditions may be shown. The following lemmas, referenced from [46], [47], will be used in the convergence proof. For simplicity we define Ω to be the feasible set of (19), and $\Omega^{[t]}$ to be the feasible set of (37) for the t^{th} iteration.

Lemma 1. Let $\mathcal{D} : \mathbb{R}^n \rightarrow \mathbb{R}$ be a strictly convex and differentiable function on a nonempty convex set $S \subseteq \mathbb{R}^n$. Then \mathcal{D} is strongly convex on the set S .

Proof. See [46]. ■

Lemma 2. Let $\{\mathbf{x}^{[t]}\}$ be the sequence generated by the SPCA method. Then, for every $t \geq 0$: **i)** $\Omega^{[t]} \subseteq \Omega$, **ii)** $\mathbf{x}^{[t]} \in \Omega^{[t]} \cap \Omega^{[t+1]}$, **iii)** $\{\mathbf{x}^{[t]}\}$ is a feasible point of (19), **iv)** $r_{sec}^{[t]} \leq r_{sec}^{[t+1]}$.

Proof. See [46]. ■

Lemma 3. The sequence $r_{sec}^{[t]}$ converges.

Proof. See [46], [47]. ■

Given the aforementioned lemmas and following the same approach as in [47], the convergence of Algorithm 1 is trivial. The convergence of Algorithm 3 can be proved similarly to the algorithm in [48]. The Algorithm 4 iterates between Algorithm 1 and Algorithm 3; thus, its convergence follows as well.

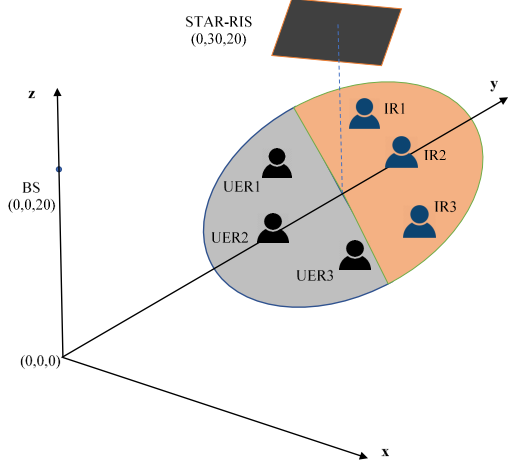


Fig. 4. Simulation scenario for the STAR-RIS-RSMA system.

B. Complexity Analysis

The complexity of Algorithm (4) depends primarily on the complexity of Algorithms (1) and (3). In Algorithm (1), the major complexity lies in the matrix multiplication of (25). Thus, the worst-case complexity order of solving the convex problem is given by $O_1 \triangleq \mathcal{O}(N_{max}(M^2 N_T)^2 \max(K, J))$, where N_{max} is the number of iterations.

Algorithm (3) for finding the transmission and reflection beamforming vectors in (58) requires on the order of $O_2 \triangleq \mathcal{O}(l_{max} \max(M, 2(K+J))^4 \sqrt{M} \log_2 \frac{1}{\epsilon_1})$ computations, where l_{max} is the number of iterations for Algorithm (3) and ϵ_1 is the solution accuracy. The overall complexity of Algorithm (4) is $\mathcal{O}(W_{max}(O_1 + O_2))$ where W_{max} is the number of iterations required for the entire algorithm.

V. SIMULATION RESULTS

In this section, we present some numerical results for our proposed framework. The simulation setting for the STAR-RIS-RSMA system is based on the following scenario, unless otherwise stated. The BS is located 20m above the ground i.e. (0, 0, 20), and the RIS is located at (0, 30, 20). There are $K = 3$ IRs and $J = 3$ UERs randomly located on the two different sides of the RIS, as depicted in Fig. 4

The distance-dependent path loss for node n is modeled as $PL_n \triangleq d_n^{-\alpha_n}$ where d_n is the distance between the RIS and the user, and the path loss exponent $-\alpha_n$ is taken from the probabilistic model of [50], which is appropriate for low-altitude RISs with a LoS link that may be blocked due to environmental obstacles. In particular, the model assumes

$$\alpha_n \triangleq \frac{\mathcal{L}_n - \mathcal{N}_n}{1 + \lambda_1 e^{\lambda_2(\phi_n - \lambda_1)}} + \mathcal{N}_n, \quad (59)$$

where α_n is composed of both LoS and non-LoS components \mathcal{L} and \mathcal{N} , respectively, $\phi_n \triangleq \frac{180}{\pi} \sin^{-1}(\frac{H_{RIS}}{d_n})$ denotes the elevation angle between the RIS and the n -th user at an aerial-to-ground distance d , while λ_1 and λ_2 are determined by the wireless environment, e.g., urban, dense urban, etc. In our

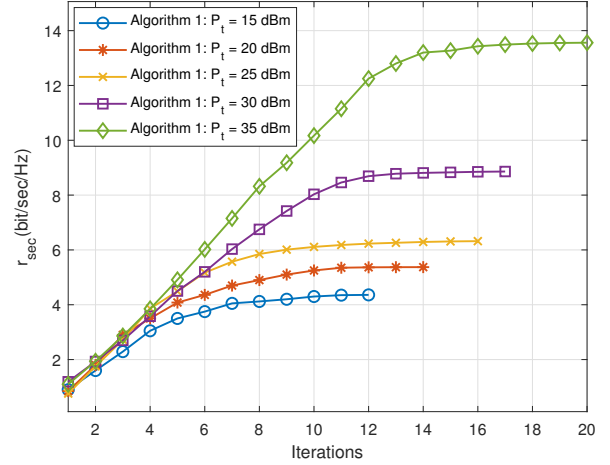


Fig. 5. Convergence behavior of Algorithm 1 versus the number of iterations for different values of transmit power when $N_T = 4$, and $M = 10$.

simulations we choose LoS and NLoS path-loss exponents of $\mathcal{L} = 2$ and $\mathcal{N} = 3.5$, respectively. The simulation results are obtained by averaging the performance over 100 channel realizations. In the algorithmic implementation, we set $N_{max} = M_{max} = 30$ and the maximum threshold value as $\delta_I = 10^{-2}$. A channel estimation error with variance of $\nu = 10^{-4}$ is assumed for the communication channel $\mathbf{g}_{r,j}$, the additive noise at the receiver side is considered to have a normalized power of 0 dBm, the minimum harvested energy needed by the UERs is $30\mu W$, and the minimum required number of common stream transmissions is $r_c = 1$.

The average convergence behavior of the proposed SPCA-based approach (Algorithm 1) is shown in Fig. 5. The curves show the secrecy rate achieved by the algorithm versus the number of iterations, and we see that increasing the transmit power leads to an improved secrecy rate at the cost of a longer convergence time. The secrecy rate improves since at some point (between 20-25 dBm) the UERs no longer need additional energy, and the SPCA method can then use the increased transmit power for improving the security of the IRs.

In Fig. 6 we consider the performance of Algorithm 1 for different values of N_T . As expected, increasing the number of transmit antennas in turn increases the number of DoFs and we achieve a higher r_{sec} . Fig. 7 investigates the convergence of Algorithm 3, and we see that the number of iterations required for attaining convergence increases with M , since more transmission and reflection coefficients have to be optimized. Moreover, we see that increasing M leads to a significant improvement in the achievable sum rate. The convergence of the overall two-step Algorithm 4 is characterized in Fig. 8, which shows rapid convergence in a small number of iterations, confirming the effectiveness of our proposed algorithm. Moreover, in high transmit power scenarios, r_{sec} increases significantly.

Fig. 9 illustrates the robustness of the proposed framework against imperfect CSIT, depicting the average worst case secrecy rate versus different levels of CSIT estimation error ν

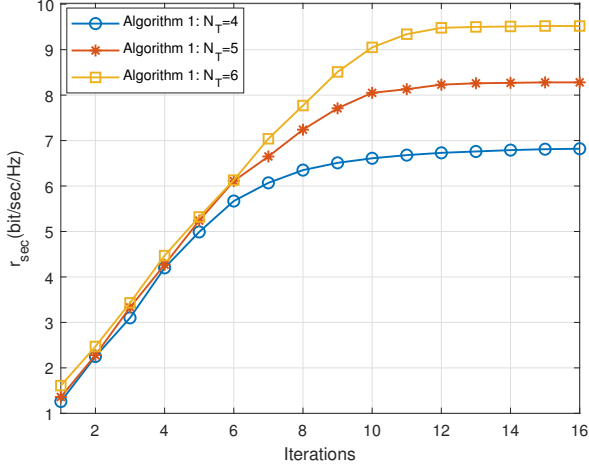


Fig. 6. Convergence behavior of Algorithm 1 for different values of N_T , when $P_t = 25\text{dBm}$ and $M = 10$.

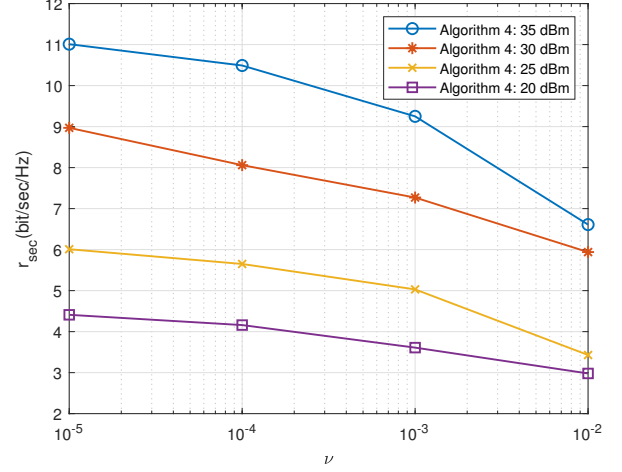


Fig. 9. Convergence behavior of Algorithm 4 versus ν parameterized by P_t when $N_T = 4$, and $M = 10$.

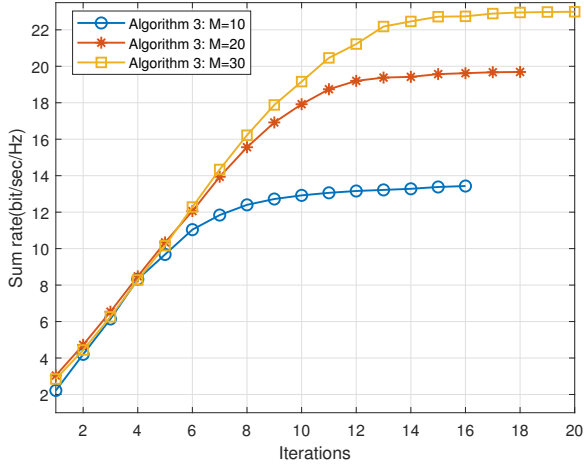


Fig. 7. Convergence behavior of Algorithm 3 for different values of M , when $P_t = 25\text{dBm}$ and $N_T = 4$.

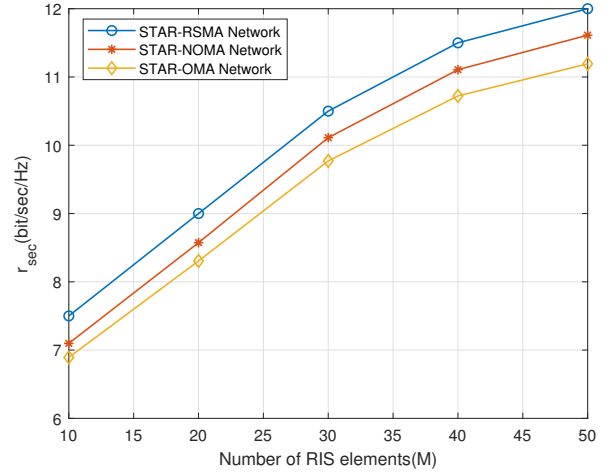


Fig. 10. Comparison of the proposed method with NOMA and OMA in STAR-RIS network.

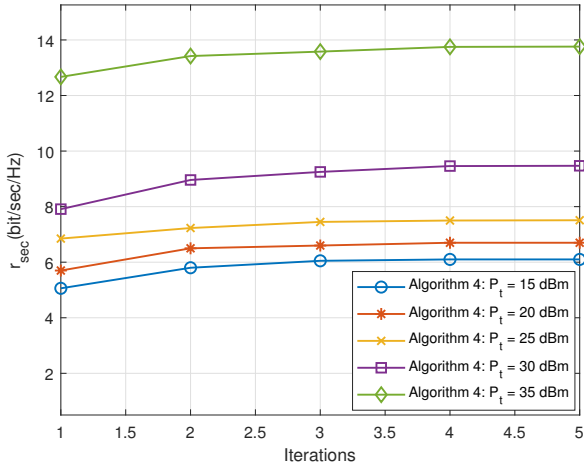


Fig. 8. Convergence behavior of Algorithm 4 versus the number of iterations for different values of transmit power when $N_T = 4$, and $M = 10$.

and transmit powers P_t . Observe that increasing ν reduces r_{sec} in all cases, although the loss can be offset by increasing P_t . In Fig. 10 we simulate the same network topology, varying only the multiplexing methods among RSMA, NOMA, and OMA. The results clearly demonstrate that the proposed strategy surpasses both NOMA and OMA, aligning with the expectations set forth in [15].

Finally, we illustrate the execution time duration (in seconds) of the overall proposed algorithm (Algorithm 4) for different numbers of users. An Intel core i5, 4 GHz processor was used and the results are presented in Table III. Observe from Table III that increasing the number of IRs and run-time of Algorithm 4. For instance, the run-time for $K = 2$ and $J = 2$ is 130s, which is approximately twice that of $K = 1$ and $J = 1$. This is because the number of constraints in Algorithm 4 depends on K and J .

TABLE III
COMPARISON OF RUN-TIME OF ALGORITHM 4 FOR DIFFERENT NUMBER OF USERS

K (N.O of IRs)	J (N.O of UERs)	run-time (s)
1	1	65s
2	1	82s
2	2	130s
3	2	168s
3	3	209s

VI. CONCLUSIONS AND FUTURE WORK

RISs are capable of improving next-generation networks. Thus, in this paper, a STAR-RIS-RSMA method was proposed for the simultaneous transmission of information and power to IRs and UERs, respectively. Since the UERs are able to wiretap the IR streams, our objective is to maximize the sum secrecy rate of the IRs under realistic constraints on the total transmit power and the energy collected by the UERs. This is achieved by jointly optimizing the precoder vectors and the RIS transmission and reflection beamforming coefficients. The formulated problem is non-convex with intricately coupled variables. In order to tackle this challenge a suboptimal two-step iterative algorithm was proposed in which the precoders and the RIS transmission/reflection beamforming coefficients are optimized in an alternating fashion. The results inferred from our simulations were used to validate the performance of the proposed method. Increasing the transmit power or the number of BS antennas improves the performance of the system. The number of STAR-RIS elements M determines the number of DoFs of the system. Thus, the results demonstrate that when M increases, the proposed method achieves higher rates. Furthermore, the proposed method converges rapidly, achieves a high secrecy rate, and shows a remarkable robustness to imperfect CSI. For ease of exposition, the quantitative results are summarized in Table IV.

In our subsequent research endeavors, we aim to conduct a thorough theoretical analysis of secure STAR-RIS networks. This will involve a deep dive into their core principles and theoretical limits to not only augment our empirical findings but also to establish a comprehensive theoretical framework guiding practical implementations. Furthermore, we plan to explore more realistic RIS models, specifically incorporating quantized reflection coefficients and a non-energy-saving model. Another significant area of future research will be addressing the challenges associated with nonlinear energy harvesting models in UERs. These expanded research directions will enable us to tackle more complex scenarios and contribute to advancing the state-of-the-art in the field.

APPENDIX A PROOF OF PROPOSITION 1

The constraint (21c) can be equivalently rewritten $\forall j \in \mathcal{J}$ as follows:

$$R_{c,j}^{\text{UER}} \leq \alpha_{c,j}, \quad \{\forall \Delta \mathbf{g}_{r,j} \in \Theta_g\}. \quad (\text{A.1})$$

TABLE IV
BRIEF REVIEW ON QUANTITATIVE RESULTS

-
- The secrecy rate achieved by Algorithm 1 improves with increasing the transmit power but results in a longer convergence time. The secrecy rate improves since for high SNRs, the UERs do not need additional energy, and the SPCA method can then use the increased transmit power to increase the security of the IRs.
-
- Increasing the number of transmit antennas increases the number of DoFs and we achieve a higher r_{sec} .
-
- Increasing the number of transmission and reflection coefficients leads to a significant improvement in the achievable sum rate as well as more complexity in Algorithm 3 with slower convergence.
-
- The two-step Algorithm 4 converges rapidly in only a few iterations, confirming the effectiveness of the proposed approach.
-
- The proposed method is robust against imperfect CSIT, with a predictable loss when the level of CSI increases. However, the loss can be compensated by increasing the transmitted power.
-

Problem (A.1) represents a search over all possible values of the channel uncertainties to find the worst-case. On the other hand, based on what we inferred earlier from (21b) and (21c), the goal is to minimize $R_{c,j}^{\text{UER}}$ by minimizing its ceiling rate $\alpha_{c,j}$. Given this fact, and with the aim of linearizing (21c), after exploiting the definition of $R_{c,j}^{\text{UER}}$ and using some variable transformations, the pair of extra auxiliary constraints becomes

$$\gamma_{c,j}^{\text{UER}} \leq \rho_{c,j} \quad (\text{A.2})$$

$$1 + \rho_{c,j} - 2^{\alpha_{c,j}} \leq 0. \quad (\text{A.3})$$

The non-convexity of (A.2) is revealed by inserting the definition of $\gamma_{c,j}^{\text{UER}}$ as well as utilizing the auxiliary variables introduced in Proposition 1. The non-convexity of (A.3) results from the term $2^{\alpha_{c,j}}$, and the non-convex factor is replaced at the i -th iteration using a first order Taylor expansion of $2^{\alpha_{c,j}}$ based on the operator $\Gamma^{[i]}(\alpha_{c,j})$. On the other hand, the problem (A.2) can be recast as follows after some trivial manipulations:

$$\frac{x_{c,j}^2}{\sum_{k' \in \mathcal{K}} a_{j,k'} + \sum_{j' \in \mathcal{J}} b_{j,j'} + 1} \leq \rho_{c,j}, \quad (\text{A.4})$$

$$\max_{\Delta \mathbf{g}_{r,j}} |\mathbf{h}_{r,j} \mathbf{p}_c| \leq x_{c,j}, \quad (\text{A.5})$$

$$\min_{\Delta \mathbf{g}_{r,j}} |\mathbf{h}_{r,j} \mathbf{p}_{k'}|^2 \leq a_{j,k'}, \quad (\text{A.6})$$

$$\min_{\Delta \mathbf{g}_{r,j}} |\mathbf{h}_{r,j} \mathbf{f}_{j'}|^2 \leq b_{j,j'}. \quad (\text{A.7})$$

In order to overcome the non-convexity of (A.5)-(A.7), we exploit the combined channel definition $\mathbf{h}_{r,j} = \mathbf{g}_{r,j}^H \Theta_r \mathbf{H}$, as well as (5), and the following proposition.

Proposition 7. For the terms $\mathcal{D}_1(\Delta \mathbf{h}) \triangleq \left| \left(\hat{\mathbf{h}} + \Delta \mathbf{h} \right)^H \mathbf{u} \right|$ and $\mathcal{D}_2(\Delta \mathbf{h}) \triangleq \left| \left(\hat{\mathbf{h}} + \Delta \mathbf{h} \right)^H \mathbf{u} \right|^2$ with norm-bounded variable $\|\Delta \mathbf{h}\|_2 \leq \sigma$, the following results hold:

$$\max_{\|\Delta \mathbf{h}\|_2 \leq \sigma} \mathcal{D}_1(\Delta \mathbf{h}) = \left| \hat{\mathbf{h}}^H \mathbf{u} \right| + \sigma \|\mathbf{u}\|_2, \quad (\text{A.8})$$

$$\min_{\|\Delta \mathbf{h}\|_2 \leq \sigma} \mathcal{D}_2(\Delta \mathbf{h}) = \text{Tr} \left[(\hat{\mathbf{H}} - \mu \mathbf{I}) \mathbf{U} \right], \quad (\text{A.9})$$

$$\max_{\|\Delta \mathbf{h}\|_2 \leq \sigma} \mathcal{D}_2(\Delta \mathbf{h}) = \text{Tr} \left[(\hat{\mathbf{H}} + \mu \mathbf{I}) \mathbf{U} \right], \quad (\text{A.10})$$

where $\hat{\mathbf{H}} \triangleq \hat{\mathbf{h}} \hat{\mathbf{h}}^H$, $\mathbf{U} \triangleq \mathbf{u} \mathbf{u}^H$, and $\mu \triangleq \sigma^2 + 2\sigma \|\hat{\mathbf{h}}\|_2$.

Proof. Please refer to [40] ■

Using Proposition 1, we can relax the right-side of (A.5)-(A.7), leading to the expressions in (25-(III))-(25-(V)).

APPENDIX B PROOF OF PROPOSITION 3

With the aim of linearizing (21g), after exploiting the definition of R_k and using some variable transformations, the two extra auxiliary constraints are formulated for $\forall k \in \mathcal{K}$, as follows:

$$1 + \rho_k - 2^{\gamma_k} \geq 0 \quad (\text{B.1})$$

$$\gamma_k^{\text{ID}} \geq \rho_k. \quad (\text{B.2})$$

To maintain the generality of the problem, the auxiliary constraints must be defined to ensure that they are active at the optimum solution. Although (B.1) is convex, substituting the definition of γ_k^{ID} into (B.2) leads to a difference of two convex functions (DC decomposition) and thus it is non-convex. The following DC decomposition is thus applied to (B.2):

$$\mathcal{M}_1(\mathbf{z}) - \mathcal{N}_1(\mathbf{z}) \leq 0, \quad (\text{B.3})$$

where $\mathbf{z} = [\mathbf{p}_k, \mathbf{f}_j, \rho_k]$, $\forall k \in \mathcal{K}, j \in \mathcal{J}$, $\mathcal{N}_1(\mathbf{z}) \triangleq \frac{|\mathbf{h}_{t,k} \mathbf{p}_k|^2}{\rho_k}$, and $\mathcal{M}_1(\mathbf{z}) \triangleq \sum_{k' \in \mathcal{K}, k' \neq k} |\mathbf{h}_{t,k} \mathbf{p}_{k'}|^2 + \sum_{j \in \mathcal{J}} |\mathbf{h}_{t,k} \mathbf{f}_j|^2 + 1$. The non-convexity of (B.2) is caused by $\mathcal{N}_1(\mathbf{z})$, as shown in (B.3), and thus the non-convex factor is replaced at the i -th iteration by a first order Taylor expansion of $\mathcal{N}_1(\mathbf{z})$ using the operator $\Psi^{[i]}(\mathbf{u}, x; \mathbf{h})$.

APPENDIX C PROOF OF PROPOSITION 5

Due to the nonlinear term $\alpha_k R_c$, (19e) is non-convex. To deal with this non-convexity, we first write the equivalent DC decomposition of (19e) as:

$$r_c + (\mathcal{A}(\alpha_k, R_c) - \mathcal{B}(\alpha_k, R_c)) \leq 0, \quad (\text{C.1})$$

where $\mathcal{A}(\alpha_k, R_c) \triangleq \frac{1}{4}(\alpha_k - R_c)^2$ and $\mathcal{B}(\alpha_k, R_c) \triangleq \frac{1}{4}(\alpha_k + R_c)^2$. As can be observed, the non-convexity of (C.1) is caused by $\mathcal{B}(\alpha_k, R_c)$. Therefore, we replace it by the affine

approximation obtained by the first-order Taylor expansion at the i -th iteration, i.e., $\hat{\mathcal{B}}^{[i]}(\alpha_k, R_c)$. Subsequently, inserting $\hat{\mathcal{B}}^{[i]}(\alpha_k, R_c)$ into (C.1), the affine approximation of (19e) is given by:

$$\Theta^{[i]}(\alpha_k, R_c) \geq r_c. \quad (\text{C.2})$$

APPENDIX D PROOF OF PROPOSITION 6

The constraint (19f) represents a search over all possible values of the channel uncertainty to find the worst-case. Using the definition of Q_j from (14) and some variable transformations, four extra auxiliary constraints emerge, as follows:

$$\sum_{j \in \mathcal{J}} \left(\lambda_{j,c} + \sum_{k \in \mathcal{K}} \lambda_{j,k} + \sum_{j' \in \mathcal{J}} \xi_{j,j'} \right) \geq E^{th}, \quad (\text{D.1})$$

$$\min_{\Delta \mathbf{g}_{r,j}} |\mathbf{h}_{r,j} \mathbf{p}_c|^2 \geq \lambda_{j,c}, \quad \forall j \in \mathcal{J}, \quad (\text{D.2})$$

$$\min_{\Delta \mathbf{g}_{r,j}} |\mathbf{h}_{r,j} \mathbf{p}_k|^2 \geq \lambda_{j,k}, \quad \forall j \in \mathcal{J}, k \in \mathcal{K}, \quad (\text{D.3})$$

$$\min_{\Delta \mathbf{g}_{r,j}} |\mathbf{h}_{r,j} \mathbf{f}_{j'}|^2 \geq \xi_{j,j'}, \quad \forall j, j' \in \mathcal{J}. \quad (\text{D.4})$$

It can be observed that (D.2)-(D.4) are still non-convex. Utilizing proposition 1 in Appendix A, the convex counterparts can be obtained as shown in (36).

REFERENCES

- [1] M. Di Renzo, A. Zappone, M. Debbah, M.-S. Alouini, C. Yuen, J. de Rosny, and S. Tretyakov, "Smart radio environments empowered by reconfigurable intelligent surfaces: How it works, state of research, and road ahead," *IEEE J. Sel. Areas Commun.*, vol. 38, no. 11, pp. 2450–2525, Nov. 2020.
- [2] Q. Wu and R. Zhang, "Towards smart and reconfigurable environment: Intelligent reflecting surface aided wireless network," *IEEE Commun. Mag.*, vol. 58, no. 1, pp. 106–112, Jan. 2020.
- [3] C. Huang, S. Hu, G. C. Alexandropoulos, A. Zappone, C. Yuen, R. Zhang, M. Di Renzo, M. Debbah, "Holographic MIMO surfaces for 6G wireless networks: Opportunities, challenges, and trends," *IEEE Wireless Commun.*, vol. 27, no. 5, pp. 118–125, 2020.
- [4] Q. Wu and R. Zhang, "Intelligent reflecting surface enhanced wireless network via joint active and passive beamforming," *IEEE Trans. Wireless Commun.*, vol. 18, no. 11, pp. 5394–5409, Nov. 2019.
- [5] Q. Wu and R. Zhang, "Beamforming optimization for wireless network aided by intelligent reflecting surface with discrete phase shifts," *IEEE Trans. Commun.*, vol. 68, no. 3, pp. 1838–1851, Mar. 2020.
- [6] Y. Liu, X. Mu, J. Xu, R. Schober, Y. Hao, H. V. Poor, and L. Hanzo, "STAR: Simultaneous transmission and reflection for 360° coverage by intelligent surfaces," *IEEE Wireless Communications*, vol. 28, no. 6, pp. 102–109, December 2021.
- [7] X. Mu, Y. Liu, L. Guo, J. Lin, and R. Schober, "Simultaneously transmitting and reflecting (STAR) RIS aided wireless communications," *IEEE Trans. Commun.*, vol. 21, no. 5, pp. 3083–3098, May 2022.
- [8] S. Zeng, H. Zhang, B. Di, Y. Tan, Z. Han, H. V. Poor, and L. Song, "Reconfigurable intelligent surfaces in 6G: Reflective, transmissive, or both?" *IEEE Commun. Lett.*, vol. 25, no. 6, pp. 2063–2067, Jun. 2021.
- [9] C. Pfeiffer and A. Grbic, "Metamaterial Huygens' surfaces: Tailoring wave fronts with reflectionless sheets," *Phys. Rev. Lett.*, vol. 110, no. 19, pp. 197401, 2013.
- [10] X. Chen, D. W. K. Ng, W. H. Gerstacker, and H.-H. Chen, "A survey on multiple-antenna techniques for physical layer security," *IEEE Commun. Surveys Tuts.*, vol. 19, no. 2, pp. 1027–1053, 2nd Quart., 2017.
- [11] Z. Kong, J. Song, C. Wang, H. Chen, and L. Hanzo, "Hybrid analog/digital precoder design for securing cognitive millimeter wave networks," *IEEE Trans. Inf. Forensics Security*, vol. 16, pp. 4019–4034, 2021.

- [12] Y. Yang, M. Ma, S. Aïssa, and L. Hanzo, "Physical-layer secret key generation via CQI-mapped spatial modulation in multi-hop wireless ad-hoc networks," *IEEE Trans. Inf. Forensics Security*, vol. 16, pp. 1322–1334, 2021.
- [13] A. Mukherjee, S. A. A. Fakoorian, J. Huang, and A. L. Swindlehurst, "Principles of physical layer security in multiuser wireless networks: A survey," *IEEE Commun. Surveys Tuts.*, vol. 16, no. 3, pp. 1550–1573, 3rd Quart., 2014.
- [14] Y. Yuan, S. Wang, Y. Wu, H. Vincent Poor, Z. Ding, X. You, and L. Hanzo, "NOMA for next-generation massive IoT: Performance potential and technology directions," *IEEE Commun. Mag.*, vol. 59, no. 7, pp. 115–121, July 2021.
- [15] Y. Mao, B. Clerckx, and V. O. Li, "Rate-splitting multiple access for downlink communication systems: Bridging, generalizing, and outperforming SDMA and NOMA," *EURASIP J. Wireless Commun. Netw.*, vol. 1, pp. 1–54, May 2018.
- [16] C. Pan, H. Ren, K. Wang, M. Elkhassan, A. Nallanathan, J. Wang, and L. Hanzo, "Intelligent reflecting surface aided MIMO broadcasting for simultaneous wireless information and power transfer," *IEEE J. Sel.*, vol. 38, no. 8, pp. 1719–1734, Aug. 2020.
- [17] Y. Zeng, B. Clerckx, and R. Zhang, "Communications and signals design for wireless power transmission," *IEEE Transactions on Communications*, vol. 65, no. 5, pp. 2264–2290, May 2017.
- [18] B. Clerckx, R. Zhang, R. Schober, D. W. K. Ng, D. I. Kim, and H. V. Poor, "Fundamentals of wireless information and power transfer: From RF energy harvester models to signal and system designs," *IEEE Journal on Selected Areas in Communications*, vol. 37, no. 1, pp. 4–33, Jan 2019.
- [19] R. Zhang and C. K. Ho, "MIMO broadcasting for simultaneous wireless information and power transfer," *IEEE Transactions on Wireless Communications*, vol. 12, no. 5, pp. 1989–2001, May 2013.
- [20] Y. Mao, B. Clerckx and V. O. K. Li, "Rate-splitting for multi-User multi-antenna wireless information and power transfer," *2019 IEEE 20th International Workshop on Signal Processing Advances in Wireless Communications (SPAWC)*, 2019.
- [21] J. Zuo, Y. Liu, Z. Ding, L. Song, and H. V. Poor, "Joint design for simultaneously transmitting and reflecting (STAR) RIS assisted NOMA systems," arXiv:2106.03001.
- [22] C. Wu, Y. Liu, X. Mu, X. Gu and O. A. Dobre, "Coverage characterization of STAR-RIS networks: NOMA and OMA," *IEEE Communications Letters*, vol. 25, no. 9, pp. 3036–3040, Sept. 2021.
- [23] Z. Zhang, J. Chen, Y. Liu, Q. Wu, B. He, and L. Yang, "On the secrecy design of STAR-RIS assisted uplink NOMA networks," arXiv:2111.02642.
- [24] C. Wu, X. Mu, Y. Liu, X. Gu, and X. Wang, "Resource allocation in STAR-RIS-aided networks: OMA and NOMA," arXiv:2111.03883.
- [25] X. Mu, Y. Liu, L. Guo, J. Lin and R. Schober, "Simultaneously transmitting and reflecting (STAR) RIS aided wireless communications," *IEEE Trans. Wireless Commun.*, vol. 21, no. 5, pp. 3083–3098, May 2022.
- [26] X. Yue, J. Xie, Y. Liu, Z. Han, R. Liu, and Z. Ding, "Simultaneously transmitting and reflecting reconfigurable intelligent surface assisted NOMA networks," arXiv:2112.01336.
- [27] P. P. Perera, V. G. Warnasooriya, D. Kudathanthirige, and H. A. Suraweera, "Sum rate maximization in STAR-RIS assisted full-duplex communication systems," arXiv:2203.04709.
- [28] H. Niu, Z. Chu, F. Zhou, and Z. Zhu, "Simultaneous transmission and reflection reconfigurable intelligent surface assisted secrecy MISO networks," *IEEE Commun. Lett.*, vol. 25, no. 11, pp. 3498–3502, Nov. 2021.
- [29] J. Liu, K. Xiong, Y. Lu, D. W. K. Ng, Z. Zhong and Z. Han, "Energy efficiency in secure IRS-aided SWIPT," *IEEE Wireless Communications Letters*, vol. 9, no. 11, pp. 1884–1888, Nov. 2020.
- [30] J. Yang, J. Xinsheng, H. Kaizhi, S. Xiaoli, and Y. Wang, "Enhanced secure SWIPT in heterogeneous network via intelligent reflecting surface," *Security and Communication Networks*, vol. 2021.
- [31] N. Hehao and L. Ni, "Intelligent reflect surface aided secure transmission in MIMO channel with SWIPT," *IEEE Access*, vol. 8, pp. 192132–192140, 2020.
- [32] Q. Wu and R. Zhang, "Joint active and passive beamforming optimization for intelligent reflecting surface assisted SWIPT under QoS constraints," *IEEE Journal on Selected Areas in Communications*, vol. 38, no. 8, pp. 1735–1748, Aug. 2020.
- [33] H. Bastami, M. Moradikia, H. Behroozi, R. C. de Lamare, A. Abdelhadi, and Z. Ding, "Secrecy rate maximization for hardware impaired untrusted relaying network with deep learning," *Physical Communication*, Volume 49, 2021.
- [34] Z. Zhang, J. Chen, Y. Liu, Q. Wu, B. He and L. Yang, "On the secrecy design of STAR-RIS assisted uplink NOMA networks," *IEEE Trans. Wirel. Commun.*, vol. 21, no. 12, pp. 11207–11221, Dec. 2022.
- [35] H. Fu, S. Feng, W. Tang, and D. W. K. Ng, "Robust secure beamforming design for two-user downlink MISO rate-splitting systems," *IEEE Trans. Wirel. Commun.*, vol. 19, no. 12, pp. 8351–8365, Dec. 2020.
- [36] E. Boshkovska, D. W. K. Ng, N. Zlatanov, A. Koelpin and R. Schober, "Robust resource allocation for MIMO wireless powered communication networks based on a non-linear EH model," *IEEE Transactions on Communications*, vol. 65, no. 5, pp. 1984–1999, May 2017.
- [37] H. Joudeh and B. Clerckx, "Sum-rate maximization for linearly precoded downlink multiuser MISO systems with partial CSIT: A rate-splitting approach," *IEEE Transactions on Communications*, vol. 64, no. 11, pp. 4847–4861, Nov 2016.
- [38] H. Joudeh and B. Clerckx, "Rate-splitting for max-min fair multigroup multicast beamforming in overloaded systems," *IEEE Transactions on Wireless Communications*, vol. 16, no. 11, pp. 7276–7289, Nov 2017.
- [39] J. Xu, L. Liu, and R. Zhang, "Multiuser MISO beamforming for simultaneous wireless information and power transfer," *IEEE Transactions on Signal Processing*, vol. 62, no. 18, pp. 4798–4810, Sep. 2014.
- [40] E. A. Gharavol, Y. Liang and K. Mouthaan, "Robust downlink beamforming in multiuser MISO cognitive radio networks with imperfect channel-state information," *IEEE Transactions on Vehicular Technology*, vol. 59, no. 6, pp. 2852–2860, July 2010.
- [41] M. Moradikia, H. Bastami, A. Kuhestani, H. Behroozi, and L. Hanzo, "Cooperative secure transmission relying on optimal power allocation in the presence of untrusted relays, a passive eavesdropper and hardware impairments," *IEEE Access*, vol. 7, pp. 116 942–116 964, 2019.
- [42] H. Bastami, M. Moradikia, H. Behroozi, R. C. de Lamare, A. Abdelhadi, and Z. Ding, "Secrecy rate maximization for hardware impaired untrusted relaying network with deep learning," [Online]. Available: <http://arxiv.org/abs/2101.02749>, 2021.
- [43] X. Mu, Y. Liu, L. Guo, J. Lin, and N. Al-Dhahir, "Exploiting intelligent reflecting surfaces in NOMA networks: Joint beamforming optimization," *IEEE Trans. Wireless Commun.*, vol. 19, no. 10, pp. 6884–6898, Oct. 2020.
- [44] X. Mu, Y. Liu, L. Guo, J. Lin, and R. Schober, "Joint deployment and multiple access design for intelligent reflecting surface assisted networks," *IEEE Trans. Wireless Commun.*, vol. 20, no. 10, pp. 6648–6664, Oct. 2021.
- [45] M. Grant and S. Boyd, "CVX: Matlab software for disciplined convex programming, version 2.1," <http://cvxr.com/cvx>, Mar. 2014.
- [46] A. Beck, A. Ben-Tal, and L. Tretuashvili, "A sequential parametric convex approximation method with applications to nonconvex truss topology design problems," *J Glob Optim* 47, 29–51 (2010).
- [47] H. Bastami, H. Behroozi, M. Moradikia, A. Abdelhadi, D. W. K. Ng and L. Hanzo, "Large-Scale Rate-Splitting Multiple Access in Uplink UAV Networks: Effective Secrecy Throughput Maximization Under Limited Feedback Channel," *IEEE Transactions on Vehicular Technology*, vol. 72, no. 7, pp. 9267–9280, July 2023.
- [48] P. Cao, J. Thompson, and H. V. Poor, "A sequential constraint relaxation algorithm for rank-one constrained problems," *Proc. Eur. Signal Process. Conf. (EUSIPCO)*, p. 1060–1064, 2017.
- [49] S. Boyd, and L. Vandenberghe, (2004). *Convex Optimization*. Cambridge: Cambridge University Press.
- [50] A. Omri and M. O. Hasna, "Physical layer security analysis of UAV based communication networks," in *Proc. IEEE 88th Vehicular Technology Conference (VTC-Fall)*, Chicago, IL, USA, Aug. 2018.